crystals

MDPI

Article

Green Synthesized Composite AB-Polybenzimidazole/TiO_2 Membranes with Photocatalytic and Antibacterial Activity

Hristo Penchev [1,*], Katerina Zaharieva [2,*], Silvia Dimova [1], Ivelina Tsacheva [1], Rumyana Eneva [3], Stephan Engibarov [3], Irina Lazarkevich [3], Tsvetelina Paunova-Krasteva [3], Maria Shipochka [4], Ralitsa Mladenova [5], Ognian Dimitrov [6], Daniela Stoyanova [4] and Irina Stambolova [4]

1 Institute of Polymers, Bulgarian Academy of Sciences, "Akad. G. Bonchev" St., Block 103A, 1113 Sofia, Bulgaria; dimova@polymer.bas.bg (S.D.); itsacheva@polymer.bas.bg (I.T.)
2 Institute of Mineralogy and Crystallography, "Acad. I. Kostov", Bulgarian Academy of Sciences, Acad. G. Bonchev St., Block 107, 1113 Sofia, Bulgaria
3 The Stephan Angeloff Institute of Microbiology, "Acad. G. Bonchev" St., Block 26, 1113 Sofia, Bulgaria; rum_eneva@abv.bg (R.E.); stefan_engibarov@abv.bg (S.E.); irinalazarkevich@abv.bg (I.L.); pauny@abv.bg (T.P.-K.)
4 Institute of General and Inorganic Chemistry, Bulgarian Academy of Sciences, "Acad. G. Bonchev" St., Bl. 11, 1113 Sofia, Bulgaria; shipochka@svr.igic.bas.bg (M.S.); dsto@svr.igic.bas.bg (D.S.); stambolova@yahoo.com (I.S.)
5 Institute of Catalysis, Bulgarian Academy of Sciences, "Acad. G. Bonchev" St., Bl. 11, 1113 Sofia, Bulgaria; ralitsa@ic.bas.bg
6 Institute of Electrochemistry and Energy Systems, "Acad. Evgeni Budevski", Bulgarian Academy of Sciences, Acad. G. Bonchev St., Block 10, 1113 Sofia, Bulgaria; ognian.dimitrov@iees.bas.bg
* Correspondence: h_penchev@polymer.bas.bg (H.P.); zaharieva@imc.bas.bg (K.Z.)

Abstract: Novel AB-Polybenzimidazole (AB-PBI)/TiO_2 nanocomposite membranes have been prepared using a synthetic green chemistry approach. Modified Eaton's reagent (methansulfonic acid/P_2O_5) was used as both reaction media for microwave-assisted synthesis of AB-PBI and as an efficient dispersant of partially agglomerated titanium dioxide powders. Composite membranes of 80 μm thickness have been prepared by a film casting approach involving subsequent anti-solvent inversion in order to obtain porous composite membranes possessing high sorption capacity. The maximal TiO_2 filler content achieved was 20 wt.% TiO_2 nanoparticles (NPs). Titania particles were green synthesized (using a different content of *Mentha Spicata* (MS) aqueous extract) by hydrothermal activation (150 °C), followed by thermal treatment at 400 °C. The various methods such as powder X-ray diffraction and Thermogravimetric analyses, X-ray photoelectron spectroscopy, Fourier transform infrared spectroscopy and Energy-dispersive X-ray spectroscopy, Electronic paramagnetic resonance, Scanning Electron Microscopy and Transmission Electron Microscopy have been used to study the phase and surface composition, structure, morphology, and thermal behavior of the synthesized nanocomposite membranes. The photocatalytic ability of the so-prepared AB-Polybenzimidazole/bio-TiO_2 membranes was studied for decolorization of Reactive Black 5 (RB5) as a model azo dye pollutant under UV light illumination. The polymer membrane in basic form, containing TiO_2 particles, was obtained with a 40 mL quantity of the MS extract, exhibiting the highest decolorization rate (96%) after 180 min of UV irradiation. The so-prepared AB-Polybenzimidazole/TiO_2 samples have a powerful antibacterial effect on *E. coli* when irradiated by UV light.

Keywords: AB-PBI/TiO_2; membrane; green synthesis; photocatalyst; decolorization; Reactive Black 5; dye; antibacterial activity; *E. coli*

check for updates

Citation: Penchev, H.; Zaharieva, K.; Dimova, S.; Tsacheva, I.; Eneva, R.; Engibarov, S.; Lazarkevich, I.; Paunova-Krasteva, T.; Shipochka, M.; Mladenova, R.; et al. Green Synthesized Composite AB-Polybenzimidazole/TiO_2 Membranes with Photocatalytic and Antibacterial Activity. *Crystals* **2024**, *14*, 1081. https://doi.org/10.3390/cryst14121081

Academic Editor: Claudia Graiff

Received: 8 November 2024
Revised: 5 December 2024
Accepted: 10 December 2024
Published: 16 December 2024

Copyright: © 2024 by the authors. Licensee MDPI, Basel, Switzerland. This article is an open access article distributed under the terms and conditions of the Creative Commons Attribution (CC BY) license (https://creativecommons.org/licenses/by/4.0/).

1. Introduction

Combining polymer materials with selected nano-scale size oxide particles enables the possibility of preparing materials with a wide spectrum of applications [1]. In the last decades, scientific efforts have been directed at seeking new types of polymer hybrid

materials that have, at the same time, enhanced photocatalytic activity for the decolorization of organic pollutants in wastewater while manifesting efficient antimicrobial properties. By controlling their composition, the size of the nano-phase, and the chemical bonding between the organic and inorganic phases, one could obtain hybrid nanocomposites possessing the desired thermal, electric, optical, mechanical, and biological properties. Such types of composites have been studied intensively in lithium-ion batteries [2], in solar and fuel cells [3,4], and in photocatalysis [5]. In medicine, nanoparticles are used as antibacterial agents in drug delivery systems and in clinical diagnosis. The composites based on polymer hybrid materials with incorporated metal nanoparticles also have strong antibacterial properties, which could be applied in the production of packages for foodstuffs and in the treatment of textile materials.

A large number of metal oxides are used as photocatalytic/antimicrobial agents, such as zinc oxide (ZnO), titanium dioxide (TiO_2), CeO_2, etc. [6]. Among them, titanium dioxide is a non-toxic, insoluble, and stable metal oxide that is extensively used in various industries due to its excellent optical, photocatalytic, antimicrobial, and anticorrosive properties.

More and more publications are appearing in the current scientific research literature connected with the application of methods of green chemistry/synthesis, leading to obtaining oxide nanoparticles that have promising photocatalytic and antimicrobial properties [7–9]. The use of plant extracts is economically beneficial (one-step preparation) because they are cheap, bioresource-based, and environmentally friendly. Biosynthesis guarantees the production of materials with improved properties compared to traditional methods. Synthesis involving plant extracts can provide preparation of stable nanoparticles of controlled size and morphology and, last but not least, reduced cytotoxicity of nanoparticles thanks to their encapsulation in a biologically inert medium [10]. Recently, the plant-mediated synthesis was successfully applied to TiO_2 particle production [11]. S.S. Muniandy et al. have synthesized an active mesoporous powder of TiO_2 using a green chemistry approach that has a high photocatalytic efficiency for dye decolorization and good catalytic activity even after repeated use [12]. Other research groups have hydrothermally synthesized TiO_2 using *Morindacitrifolia* leaf extract, which shows promising activity against fungal pathogens and bacteria, both Gram-positive and Gram-negative strains [13].

The advancement of heterogeneous photocatalysis in various fields, such as decolorization of Methylene blue dye using Ni-doped ZnO nanostructures [14], decontamination of Cr(VI) and norfloxacin antibiotic using Au/MIL-101(Fe)/BiOBr photocatalyst [15], etc. has been discussed in the literature.

During the last few years, studies on the photocatalytic properties of hybrid nanocomposites have become the hot topic of the day on the basis of polymer/inorganic oxide composite materials in different forms for the purification of model pollutant dye-contaminated waters. The electron- and ion-conducting polymers, which most often have aromatic conjugated structures and metal oxides, possess good electron donor properties under the effect of light. The photocatalysts make use of the light energy, whereupon electron–hole pairs are formed, generating free radicals, which are involved in the reactions for demineralization of stable, persevering toxic compounds. In order to overcome the limitations, due to the fast recombination of the electron–hole pairs, the conjugated polymers are combined with semiconductor oxide nanoparticles of dimensions of about 2–10 nanometers. In such mixtures, the organic polymer acts as a donor of electrons, while the inorganic nanoparticles are electron acceptors [16].

TiO_2–polymer composites in membrane form are among the most often used in water purification and wastewater treatment [17]. The various polymers, such as polyacrylonitrile (PAN) [18], poly(vinylidene fluoride) (PVDF)/sulfonated polyethersulfone (SPES) [19], polyamide [20], polyvinylidenefluoride (PVDF) [21], polyethersulfone (PES) [22], polyurethane (PU) [23], polyethyleneterephthalate (PET) [24], polyester [25], poly(vinylidene fluoride) [26], and polytetrafluoroethylene (PTFE) [27], have been investigated as support membranes of photocatalysts.

Among them, the aromatic polybenzimidazoles (PBIs) group of heterocyclic high-performance polymers has been studied as an attractive candidate for the preparation of hollow fiber membranes used in liquid and gas separations. Some of these membranes have achieved industrial requirements under extremely harsh process environments (i.e., high temperatures, chlorine, organic solvents, and extreme pH values) due to their robust mechanical stability, structural rigidity, and outstanding chemical resistance [28]. Justo Lobato's research group prepared several TiO_2/meta-PBI-based composite membranes for application in high-temperature, solid-state polymer electrolyte membrane fuel cells [29,30] and for green hydrogen production [31–33]. In a short communication, Penchev et al. revealed, for the first time, the preparation of some novel meta- and AB-PBI-based hybrid materials with in situ synthesized ZnO NPS in the form of powders and thin films and studied their photocatalytic activity towards Malachite green as a model dye contaminant [34].

The fight against infectious diseases is complicated due to the natural ability of microorganisms to adapt themselves and bypass the antimicrobial activity of a wide range of preparations. The application of antimicrobial polymers is a novel approach to overcome these limitations [35–38]. It has several advantages, as these products typically exhibit long-term activity and limited residual toxicity, they are chemically stable, non-volatile, and they do not penetrate the skin [39]. The antimicrobial features of TiO_2 particles have been studied and described in a large number of experimental and review studies [40–44]. It has been established that the formation of reactive oxygen species (ROS), similar to other metal oxides, leads to damage and destruction of microbial cells [45,46]. The data on the ability of titanium dioxide NPs to produce ROS in the dark and under irradiation are contradictory. Some publications report the presence of ROS only under UV light exposure, while others detect ROS both in the dark and upon irradiation. It is possible that these differences are due to the different methods used to prepare the nanoparticles, their different sizes, surface defects, and the conditions of the experiments [46,47]. The use of herbs, which have enhanced antibacterial and antioxidant properties, also has advantages, resulting in an improvement in the antimicrobial activity and a decrease in the cytotoxicity of the obtained TiO_2 particles.

According to our knowledge, the preparation of AB-PBI/TiO_2 membranes and the study of their photocatalytic/antimicrobial properties is still missing in the literature. The aim of this study is to evaluate the UV-initiated photocatalytic activity for Reactive Black 5 (RB5) azo dye decolorization, as well as the antibacterial activity towards *E. coli* (under dark and UV conditions), of the novel composite AB-PBI membranes containing TiO_2 particles, produced with different contents of *Mentha Spicata* plant extract.

2. Materials and Methods

2.1. Materials

3,4 diaminobenzoic acid (97%, Merck) (DABA), methanesulfonic acid (98%, Merck), and phosphorous (V) oxide (98%, Alfa Aesar) were used as received. Titanium (IV) isopropoxide (Alfa Aesar, Haverhill, MA, USA); acetic acid (Valerus, Sofia, Bulgaria); acetyl acetone (Sigma Aldrich, Saint Louis, MO, USA ReagentPlus, ≥99%); isopropanol (Sigma Aldrich, Saint Louis, MO, USA); Mentha Spicata leaves (Bulgarian ecological region); Reactive Black 5 (Sigma Aldrich, Saint Louis, MO, USA), dye content ≥50%; hydrochloric acid 37%, p.a. analytical reagent (Valerus, Sofia, Bulgaria).

2.2. Bio-Mediated TiO_2 Particles

Mentha Spicata (MS) is a plant that belongs to the family Lamiaceae. It is widely used in medicine, pharmacy, etc., due to its excellent antimicrobial and antioxidant properties. A Mentha Spicata-mediated green approach, combined with hydrothermal treatment, was used to obtain titanium dioxide nanoparticles. The MS leaves were washed and dried, and afterward, they were ground into powder and mixed with double-distilled water. In order to obtain the final extract, the solution was heated up, then it was centrifuged and filtered. The titanium precursor solution was prepared using Ti isopropoxide, acetic acid,

and acetyl acetone (complexing agent) dissolved in isopropanol. The evaluated quantities of the as-prepared MS extract were added to the Ti solution. The resulting mixture was transferred into an autoclave at 150 °C. The as-obtained precipitates were washed and then dried in an oven, and thereafter, they were treated thermally at 400 °C for 3 h. Powders prepared from solutions having 40 mL MS, 70 mL MS, and 100 mL MS extracts are denoted as M0, M1, and M2, respectively.

2.3. Preparation of AB-PBI/Bio-TiO_2 Membranes

The incorporation of TiO_2 M0, M1, and M2 particle powders into the polybenzimidazole matrix was performed by in situ polycondensation of DABA monomer in the presence of anatase particles of 20 wt.% content, according to the theoretical total polymer concentration after polymerization, resulting in AB-PBI/TiO_2 composite stock solutions used further for the membrane preparation. In a typical procedure in a 50 cm^3 three-neck flask supplied with a magnetic stirrer, 2.1 g of DABA was dissolved by vigorous stirring in 30 g Eaton's reagent for 2 h at 70 °C under an argon atmosphere until full dissolution of the monomer. Next, 0.3 g of TiO_2 M0, M1, or TiO_2 M2 powders were mixed in the pre-polymerization solution of DABA with a short (5 min) pulsed ultrasonic treatment for best dispersion. In the convenient heating experiments, the TiO_2 M1 and M2 particles dispersion stock solutions were gradually heated up in a silicone oil bath and left for 48 h at 140 °C till viscous polymer composite dispersion was obtained, ready for film casting. In the microwave-assisted approach, the same composite pre-polymerized stock dispersions were heated in a ROTO SYNTH Rotative Solid Phase microwave reactor from Milestone, Bergamo, Italy, for 1 h at 100 Watts irradiation power, resulting in stable viscous AB-PBI/TiO_2 dispersions as well. Composite AB-PBI/TiO_2 membranes were prepared using the inverse precipitation technique. The heated stock dispersions of TiO_2 M0, M1, and TiO_2 M2 were first film cast using a doctor's blade with a 200 μm knife gap onto a glass substrate. Immediately after the film casting, the glass substrate was poured into cold water, acting as a PBI precipitation bath. After several minutes of staying in the water bath, the inverse composite membranes self-peeled off from the glass and were poured for 12 h into a 2 L glass beaker filled with 5 wt.% ammonia solution under stirring in order to neutralize the remaining acids ionicly bonded in the AB-PBI matrix. The so neutralized AB-PBI/TiO_2 20 wt.% composite gel membranes were finally washed overnight in deionized water in order to remove the remaining ammonia and its acid salts. The dry content of the composite membranes was determined to be 6.4 wt.% gravimetrically after vacuum drying a certain amount of the surface filter paper-soaked inverse membrane, and this value is close to the theoretically estimated value.

2.4. Physicochemical Characterization of Prepared AB-PBI/Bio-TiO_2 Membranes of Bio-Synthesized TiO_2 Particles

The phase composition and particle morphology of the samples were monitored using Transmission Electron Microscopy (TEM) investigations by means of a JEOL 2100 transmission electron microscope (JEOL, Tokyo, Japan) and a JEOL 2100 XEDS: Oxford Instruments, X-MAXN 80 T CCD Camera ORIUS 1000, 11 Mp, GATAN. The X-ray photoelectron spectroscopy (XPS) was carried out using an AXIS Supra electron-spectrometer (Kratos Analitycal Ltd., Manchester, England, AlKα radiation; photon energy of 1486.6 eV). The areas and binding energies (accuracy of ±0.1 eV) of C1s, O1s, and Ti2p photoelectron peaks were monitored. UV-vis diffuse-reflectance spectroscopy (DRS) was applied to determine the band gap energy, e.g., of TiO_2 green synthesis. The diffuse-reflectance spectra (DRS) were recorded on a Thermo Evolution 300 UV-VIS spectrometer (Thermo Fisher Scientific, Waltham, Massachusetts, USA) within the wavelength range of 190 nm up to 1100 nm. Electronic paramagnetic resonance spectra (EPR) were recorded at room temperature by a JEOL JES-FA 100 EPR spectrometer (JEOL Ltd., Tokyo, Japan) operating within the X-band using a standard TE011 cylindrical resonator at a modulation frequency of 100 kHz and microwave power of 3 mW.

2.5. Physicochemical Characterization of Prepared AB-PBI/Bio-TiO_2 Membranes

The powder X-ray diffraction (PXRD) analysis was performed on an X-ray powder diffractometer "Empyrean" (Malvern Panalytical, Almelo, The Netherlands) within the range of 2θ values between 3° and 100° using Cu Kα radiation (λ = 0.154060 nm) at 40 kV and 30 mA. The presence of phases was determined using High Score Plus, Version 4.9 (4.9.0.27512) software. The average crystallite size (D), lattice strain (ε), and unit cell parameter (a) of the titanium dioxide phase were determined using the Powder Cell software [48] and using the Williamson–Hall equation [49]:

$$\beta \cos\theta = 0.9\ \lambda / D + 4\varepsilon \sin\theta \quad (1)$$

where ε is the value of internal strain, β is the full-width half-maximum (FWHM) of diffraction, θ is the Bragg's angle, λ is the wavelength of the X-ray beam used, and D is the mean crystallite size of the phase under study.

The X-ray photoelectron spectroscopy (XPS) measurements were performed using a VG ESCALAB II electron spectrometer (Birches Industrial Estate, Sussex, UK equipment) with AlKα radiation at an energy of 1486.6 eV. The binding energies were determined with an accuracy of ±0.1 eV utilizing the C1s line at 285.0 eV (from an adventitious carbon) as a reference. The chemical compositions of the films were investigated on the basis of areas and binding energies of C1s, O1s N1s, P2p, Na1s, and Ti2p photoelectron peaks (after linear subtraction of the background) and Scofield's photoionization cross-sections.

Electronic paramagnetic resonance spectra (EPR) were performed at room temperature using a JEOL JES-FA 100 EPR spectrometer operating within the X-band using a standard TE011 cylindrical resonator at a modulation frequency of 100 kHz and microwave power of 3 mW.

Fourier transform infrared (FTIR) spectroscopic analysis was carried out on an IR Affinity-1 spectrophotometer (Shimadzu, Kyoto, Japan) equipped with a MIRacle ATR accessory (diamond crystal, the depth of penetration of the IR beam into the material is 2 μm).

The surface morphology of the membranes was studied by applying scanning electron microscopy (SEM) using a Zeiss Evo 10 microscope (Carl Zeiss Microscopy, Oberkochen, Germany). The images were taken in secondary electrons and backscattered electrons mode at an accelerating voltage of 25 keV, and no conductive coating was present on the samples. The chemical composition of the surface was studied using the electron dispersive spectroscopy (EDS) probe Oxford Ultim Max 40 (Oxford Instruments, Abingdon, UK). The results were compiled with AZtec software (version 6.1 HF4).

In order to perform the scanning electron microscopy analysis, a bacterial suspension of the strain *Escherichia coli* ATCC 25922 was prepared in the same manner as that for the antimicrobial activity tests. After an incubation period, the tested membranes were washed threefold with PBS, then fixed with 4% glutaraldehyde in 0.1 M Na cacodylate buffer (pH 7.2) during the incubation period for 2 h at 4 °C. The post-fixation procedure was carried out for 1 h in a solution of 1% OsO_4 again at 4 °C. The last steps were dehydration in a graded ethanol series during 15 min time intervals and sputtered with gold using a vacuum evaporator (Edwards, Irvine, CA, USA). Observations were made on a Lyra/Tescan scanning electron microscope (TESCAN GROUP a.s., Brno, Czech Republic) with an accelerating voltage of 20 kV.

The thermogravimetric (TG) analyses were performed in an argon atmosphere on a TGA-4000 PerkinElmer instrument (PerkinElmer, Waltham, MA, USA) (temperature range 40–800 °C, 10 °C/min, nitrogen atmosphere).

2.6. Photocatalytic Activity Tests

The photocatalytic decolorization of Reactive Black 5 dye as a model contaminant at an initial concentration of aqueous solution of the dye—5 ppm—has been studied. The synthesized AB-PBI/bio-TiO_2 membranes functioning as photocatalysts were tested. The

UV-A illumination lamp, which had maximum emission at 365 nm, power of 18 W, and illumination intensity of 2.6 mW/cm^2, was used. The UV irradiation dosage for 180 min of exposure was 3.921 $\times$ 10^{-17} J/m^2. The distance of illumination between the photocatalytic reactor and the lamp was 10 cm. The photocatalytic activity tests were performed at pH = 3, adjusted by 1M HCl. The photocatalytic experiments were carried out in a semi-batch slurry photocatalytic reactor equipped with two frits blowing tiny bubbles of air (continuous flow) in order to saturate the solution in dissolved oxygen using 3 $\times$ 3 cm AB-PBI/bio-TiO_2 membranes as a photocatalyst and 75 mL (batch) of dye solution under a constant stirring rate (400 rpm). In the tested systems, the dye solution and photocatalyst were stirred in the dark for about 30 min before switching on the UV irradiation for 3 h in order to reach the adsorption–desorption equilibrium state. The investigations of the photocatalytic abilities of synthesized hybrid membranes were carried out by taking aliquot samples of the suspension out of the reaction vessel at regular time intervals. The reaction course was monitored by a UV–vis absorbance spectrophotometer UV-1600PC (VWR International, Radnor, PA, USA) within the wavelength range from 200 to 800 nm (λmax = 599 nm for RB5). The degree of decolorization was determined using dependence $((C_0 - C)/C_0) \times 100$, where C_0 and C are, respectively, the initial concentration before turning on the illumination and the residual concentration of the dye solution after illumination in the course of a given time interval.

2.7. Antibacterial Properties

Media dia and test microorganisms

For the preparation of standardized bacterial cell suspensions and the cell number counting, Mueler–Hinton Broth (MHB) and Mueler–Hinton Agar (MHA) (HiMedia Laboratories, Mumbai, India) were used. Samples of the obtained materials, including the three types of TiO_2 nanopowders (M0, M1, M2), AB-PBI membrane, and AB-PBI/M0, AB-PBI/M1, and AB-PBI/M2 composites were autoclaved at 110 °C for 15 min. *Escherichia coli* ATCC 25922 and *Bacillus subtilis* ATCC 6633 were used for Minimum inhibitory concentration (MIC) testing. The photocatalytic activity was tested on *Escherichia coli* ATCC 25922.

MICs were tested by the Resazurin-based Microtitre Dilution Assay (RMDA) as previously applied by Sarker et al. (2007) [50] under static and dynamic conditions (on a rotary shaker, 120 rpm). The initial concentrations of the starting suspensions were 5 and 20 mg/mL for each nanopowder in distilled water. They were vortexed and sonicated before use.

The antimicrobial activity of the composite membranes was tested according to the ASTM method E 2149–10 [51], adapted for a 24-well sterile plate.

Photocatalytic Antibacterial Activity of Bare and PBI-Stabilized TiO_2 Nanoparticles

For the photocatalytic antibacterial test, a standardized cell suspension of *E. coli* containing approximately 1.5 ÷ 3.0 $\times$ 10^6 cells in sterile saline was used. The applied procedures were described earlier [52].

All antibacterial tests were performed in three replicates.

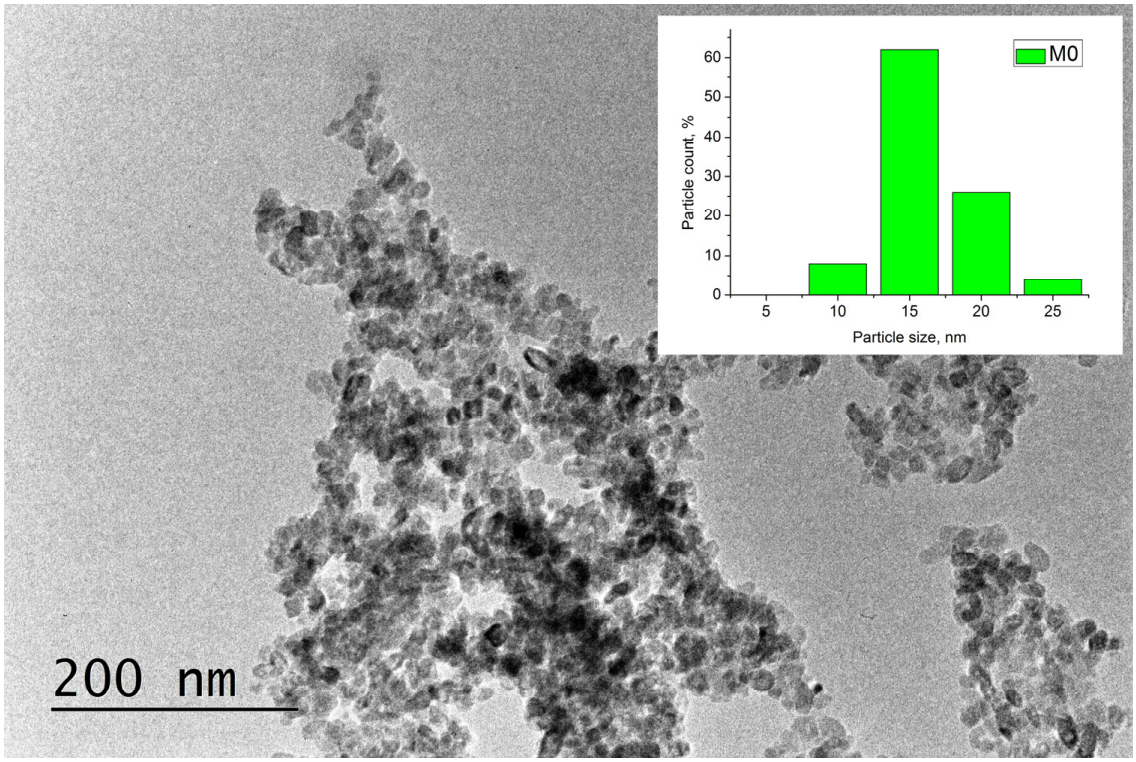
3. Results

3.1. TiO_2 Particles

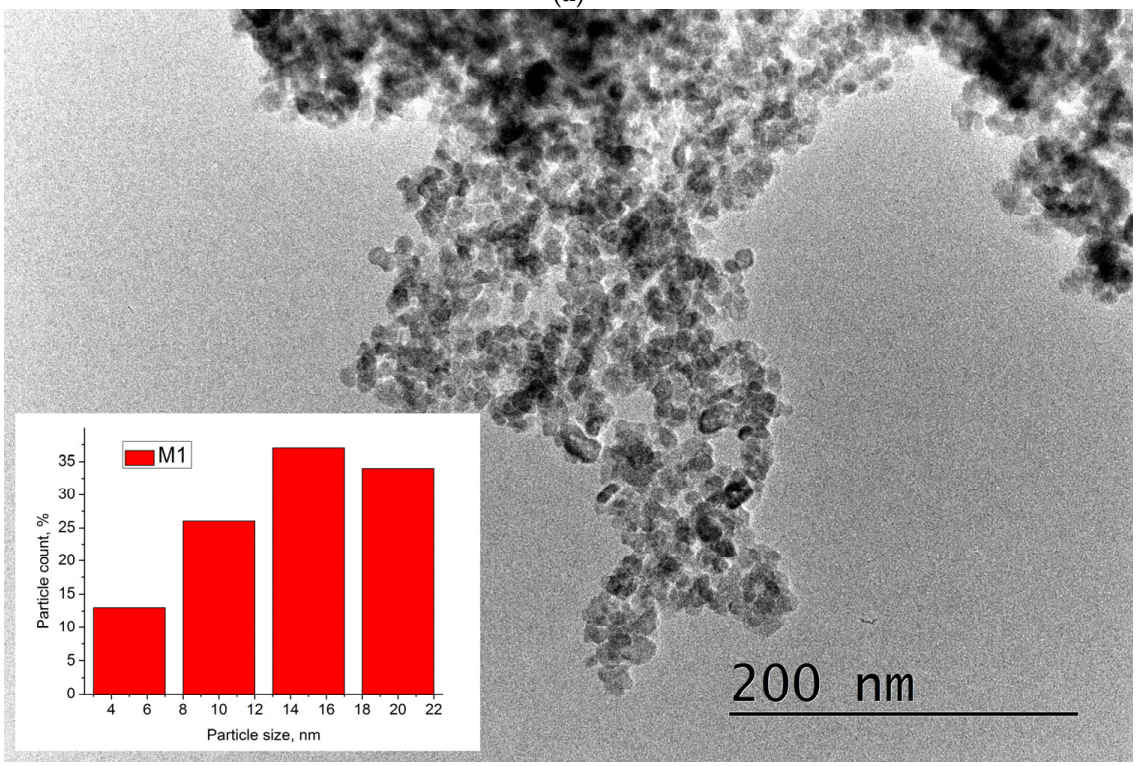
TEM micrographs show that the powders have mostly spherical morphology. The particle sizes of MO samples are within the range of 15–20 nm (Figure 1). It must be noted that the M1 powders exhibit a more homogeneous distribution than that of M0 and M2. Most of the particle sizes vary between 8 and 20 nm. For sample M2, it is characteristic that 50% of the spherical particles have a size of 15 nm, but some single smaller and bigger particles also occur.

The chemical compositions of the nanoparticles, evaluated by means of XPS analyses, are shown in Table 1. The ratio O_T/O_L increases slightly upon increasing the plant extract

quantity in the precursor solution. This fact indicates an increased number of oxygen vacancies inside the TiO_2 lattice.

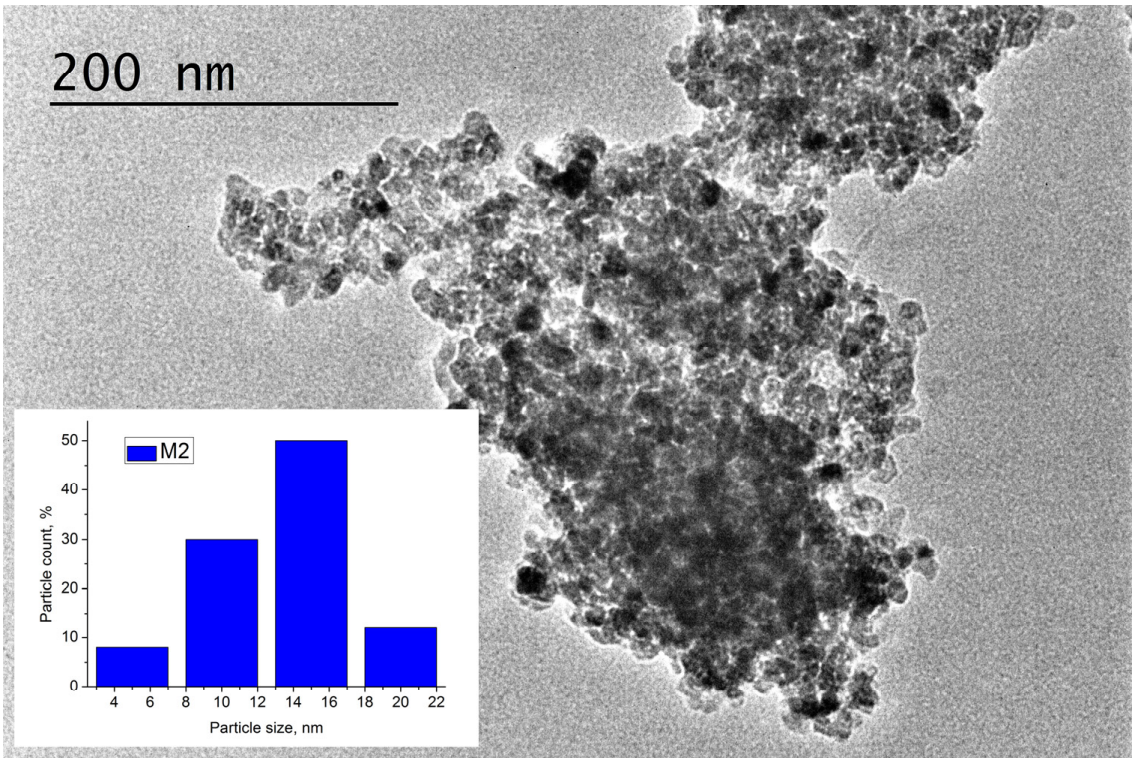


(**a**)



(**b**)

Figure 1. *Cont.*



(**c**)

Figure 1. TEM micrographs and particle size distribution of M0 (**a**), M1 (**b**), and M2 (**c**) particles.

Table 1. Chemical composition of green synthesized TiO_2 particles, evaluated by XPS analyses.

	C, at.%	O, at.%	Ti, at.%	O_T/O_L
MO	22.1	54.1	23.8	1.49
M1	20.4	56.8	22.8	1.56
M2	21.7	55.8	22.5	1.85

Note: O_T—total oxygen; O_L—lattice oxygen.

The optical properties of the green synthesized TiO_2 were investigated by DRS analyses (Figure 2). The absorption edge of the MO sample is 380 nm, while edges for M1 and M2 possess slightly lower values (Figure 3). A Kubelka–Munk transformation was used to obtain the band gap value (Figure 3). Figure 4 represents Tauc's types of plots and the estimated band gap values. From the extrapolation of the linear section of the graph $\mathbf{(h\nu F(R\infty))^{1/n}}$ from hν, the value of the optical bandgap is determined, which for pure TiO_2 is 2.98 eV, and with the addition of mint, regardless of its amount, it shifts to a higher eV value.

In Figure 5, the EPR spectra of green synthesized TiO_2 particles are shown. The signal S1 at g = 2.000 could be attributed to the presence of oxygen radicals [53,54]. The signals at g < 2 can be due to the capture of an electron on titanium ions. The broad EPR line (S3) at g = 1.93 indicates the formation of Ti^{3+} species on surface sites, while the narrow EPR signal (S2) at $g_{\perp}$= 1.991 and g// = 1.976 are probably assigned to inner electron traps (Ti^{3+}) of the particle [55]. The signal S4 at g = 2.054 can be assigned to adsorbed water or absorbed oxygen O^{2-} [54,55]. Chloride ions can react with the hole to form Cl• atoms with EPR signals at g = 2.063 (S5) and 1.997, which can originate from the plant extract (proved by EDX analysis). The signal S6 at g = 2.07 can be due to OH• radicals adsorbed on the surface [53]. When the MS concentration increases, the intensities of these EPR signals, which are attributed to the presence of Ti^{3+} and oxygen radicals, increase. Probably, the ability of plant compound constituents to reduce the metal cations is responsible for the

presence of Ti^{3+} ions. According to the research of Liu et al., the use of acetic acid in the hydrothermal process can destroy the Ti-O bond and finally form surface oxygen vacancies and Ti^{3+} [56].

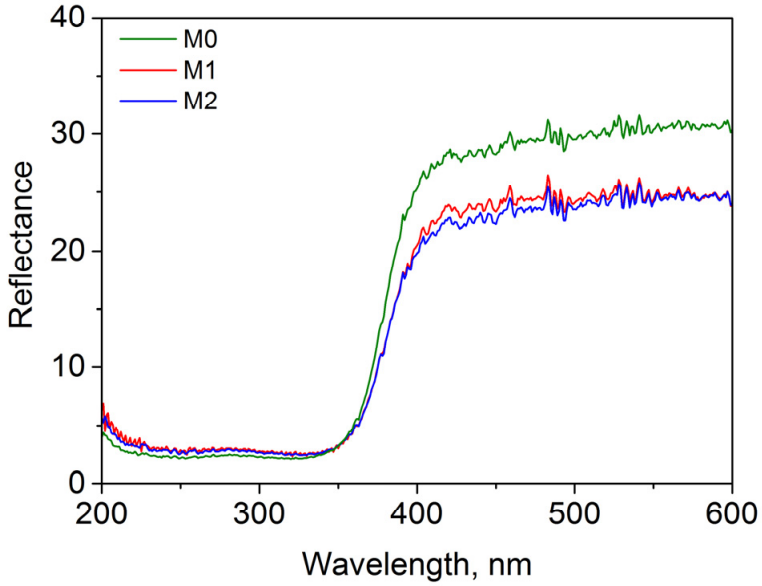


Figure 2. Diffuse-reflection spectra of green synthesized TiO_2 particles.

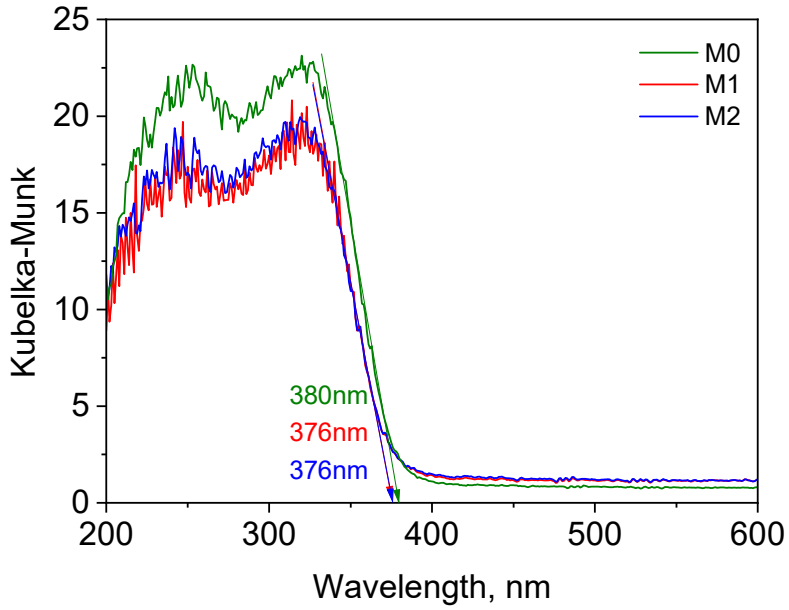


Figure 3. Absorption spectra of the green synthesized TiO_2 particles with Kubelka–Munk conversion.

The physicochemical features of the obtained plant-synthesized titania particles, nanocrystalline anatase structure, oxygen radicals, and Ti^{3+} ions decreased the band gap value, making them suitable for possible applications in the fields of catalysis or photocatalysis.

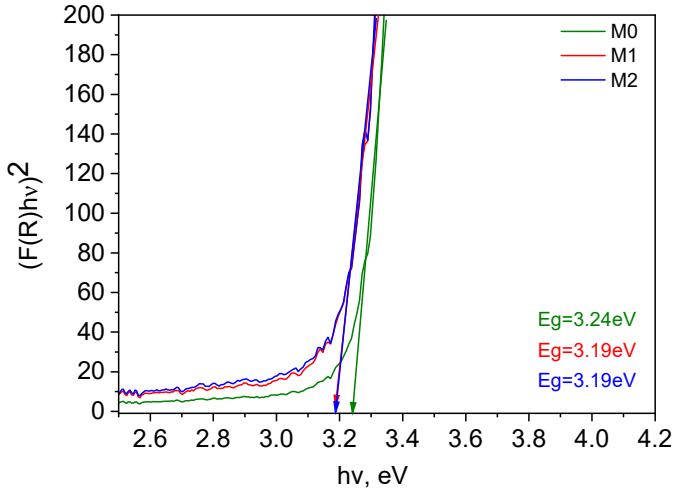


Figure 4. Tauc's plots of green synthesized TiO_2 particles.

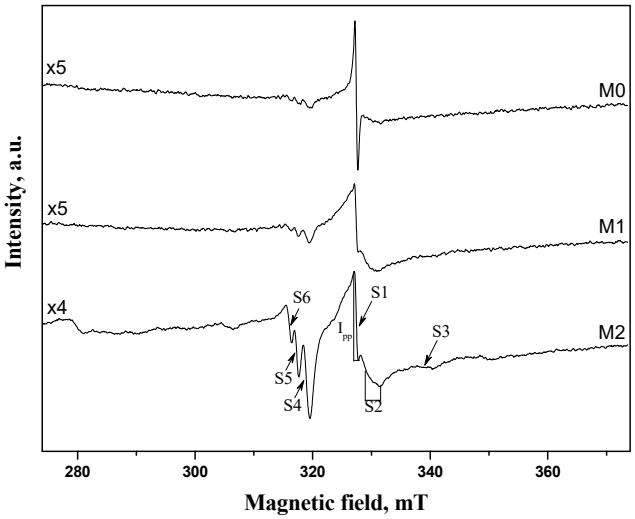


Figure 5. EPR spectra (right) of green synthesized TiO_2 particles.

3.2. Preparation of AB-PBI/Bio-TiO$_2$ Membranes

The synthetic approach for the synthesis of Poly(2,5-Benzimidazole), commonly known as AB-PBI, includes performing non-equilibrium polycondensation of single monomer 3,4 diaminobenzoic acid in modified Eaton's reagent (10 wt.% P_2O_5 dissolved in methanesulfonic acid), acting both as a dehydrating agent as well as polymer/TiO_2 particles and a solvent/dispersant, compared with the use of conventional and microwave-assisted heating at 140 °C. AB-PBI is the structurally simplest member of the PBIs group of high-performance, chemically stable, and nonflammable polymers, and it possesses the highest imidazole ring density as a repeating unit in its macromolecular backbone as well as the highest degree of crystallinity [57,58]. A very important feature of AB-PBI is the fact that it is green synthesized based on the use of a single monomer–3,4 diaminobenzoic acid, which is a cheap and low-toxicity alternative to the very expensive and cancerogenic diaminobenzidine co-monomer used in the commercial meta- and para-PBI synthetic approaches, such as the Marvel–Vogel bulk melt polycondensation [59] and that originally developed by Benicewicz et al. using a PPA sol-gel method for the para-PBI [60,61]. We had a particular challenge in our effort to incorporate well-dispersed TiO_2 particles into the AB-PBI matrix. Titania particles in different forms are known for their high-agglomeration tendency when obtained ex situ in a dry powder form [62,63]. In that aspect, we found the performance of in situ DABA polycondensation in Eaton's reagent containing well-dispersed TiO_2 particles to be a particularly useful approach. The strong polarity and in situ dehydrating power of

Eaton's reagent helped to achieve good de-agglomeration of the pristine TiO_2 powders, as well as the step-growth polymerization of DABA and the formation of a shear viscosity AB-PBI solution acting as a surface stabilizing agent. A particular reason for the use of Eaton's reagent as the polymerization medium is the solubility limitation of high-molecular AB-PBI, which is known to be poorly soluble in organic solvents traditionally used for other biphenyl-based PBIs such as dimethylacetamide/LiCl mixture [64]. We found the other reaction solvent alternative, e.g., polyphosphoric acid (PPA), particularly inappropriate for its inherent high shear viscosity and the requirement of high-power stirring. Also, the synthesis of AB-PBI in PPA solution, from our experience, results in solutions that are too viscous, which creates difficulties in film casting and obtaining membranes with poor mechanical properties.

The general synthetic procedure for AB-PBI/TiO_2 composite membrane preparation is represented in Figure 6. In recent years, the use of the microwave irradiation (MW) approach for the synthesis of high-performance polymers, including different PBIs, has gradually emerged [65,66]. It is known from the practice that the use of the MW technique permits a significant reduction of the reaction time interval, and it even results in higher molecular weight meta-PBI type polymers with the use of Eaton's reagent as a solvent and reaction medium, compared with the conventional heating technique [67]. In the present study, we employed (based on our knowledge) for the first time one pot MW and conventional heat synthesis of composite AB-PBI/TiO_2 stock dispersions using three different plant extract-synthesized anatase particles of 20 wt.% loading, as well as blank experiments based on the synthesis of pure AB-PBI with the use of Eaton's reagent. A significant reduction of reaction time interval was observed in both cases using MW irradiation, achieving high viscosity polymer solutions useful for further film casting within a 30–60 min (AB-PBI/TiO_2–pure AB-PBI) reaction time period of polycondensation being performed. The conventional heating approach, as a comparison, required a minimum 24 h reaction time period for achieving proper viscosity solutions and a high degree of imidazole cyclization for the preparation of high-molecular AB-PBI membranes possessing good physicomechanical properties. We observed a slight reduction of the apparent viscosity of the final composite AB-PBI/TiO_2 dispersions compared with the pristine PBI solutions in both cases. It could be attributed to the inherent viscosity modulation properties of the anatase nanoparticles/agglomerates phase on one side and to the kinetic polycondensation influence and side reactions on the other side. A detailed study of this observation will be the subject of further detailed investigations. An interesting UV illumination apparent color response of the pristine composite stock solution before and after aqueous membrane inversion was observed as well, which could be attributed to the complex TiO_2/AB-PBI interphase and solvent environment interactions. During the membrane water inversion process, different physicochemical changes occur both in the titania phase surface and in the polymer matrix, such as degree of protonation, hydrolysis of remaining P_2O_5, concentrated acid hydration, etc. Three different AB-PBI/20 wt.% plant extract TiO_2 composites, as well as pristine AB-PBI membranes, were prepared by film casting/direct water inversion methodology, resulting in self-supporting acid-doped hydrogel membranes with an average thickness of 80 microns. In order to remove the remaining surface mineral acid residues ionically bonded to the PBI matrix and to the titania particles from the reaction media (methane sulfonic and ortho-phosphoric acids), the obtained inverse membranes were further neutralized with basic ammonia solution, and finally, they were washed with deionized water in order to remove any remaining salt impurities within. This was performed with the presumption that deprotonated Brønsted acids could act as free radical scavengers, and this could have a negative effect on photocatalytic properties investigations and could also interfere with the antimicrobial properties interpretation. The very high chemical stability of titania anatase particles in the highly acidic reaction media was also a very useful property and it makes this kind of composite material preparation feasible.

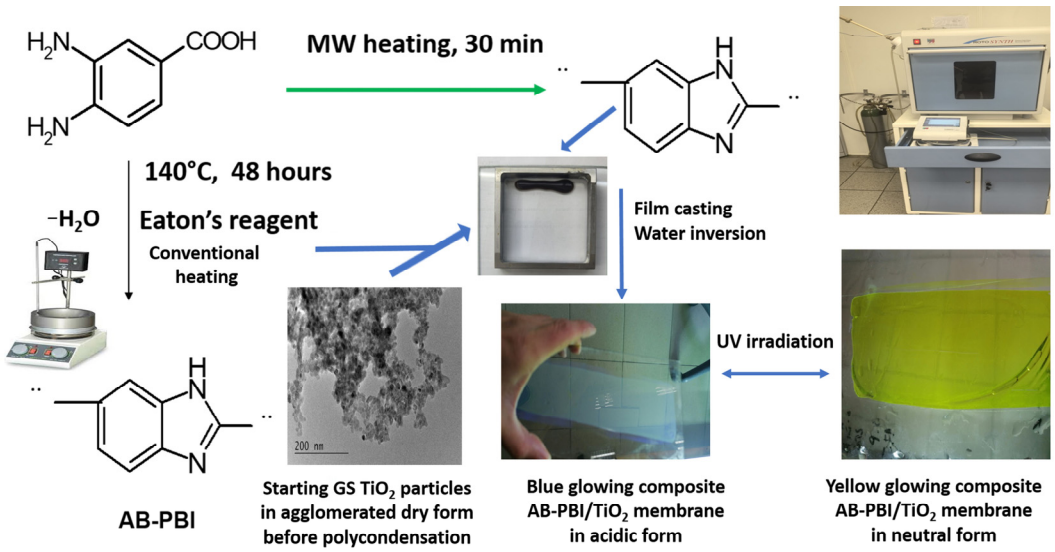


Figure 6. General preparation scheme for the synthesis of composite AB-PBI/TiO_2 membranes and reaction parameter comparison of the conventional (**left**) and microwave-assisted approaches (**right**).

3.3. Characterization of Prepared AB-PBI/Bio-TiO_2 Membranes

3.3.1. XRD Study

The powder X-ray diffraction patterns of the green synthesized TiO_2 and AB-PBI/bio-TiO_2 membranes are displayed in Figure 7. The existence of the anatase TiO_2 phase (Ref. Code: 01-083-5914) was registered in pristine titanium dioxide and AB-PBI/ bio-TiO_2 membranes. The crystallinity peaks of AB-PBI are also registered for all hybrid membranes [68]. The calculated average crystallite size, lattice microstrain parameter, and unit cell parameter of the TiO_2 phases for pure bio-synthesized TiO_2 samples (M0, M1, and M2) are 11.98 nm, 11.53, and 11.48 nm; 1.37 × 10^{-3} a.u., 2.06 × 10^{-3} a.u., and 2.13 × 10^{-3} a.u.; a: 3.783 Å, 3.786, and 3.784 Å, respectively. The higher content of the plant extract leads to a slight decrease in the crystallite sizes of the obtained particles. Similar results about decreasing particle sizes of bio-synthesized ZnO using different amounts of neem leaf extract were established by [69]. This could be due to the phytochemicals in the leaf extract, which not only act as a stabilizing agent but also as a powerful reducing agent [69].

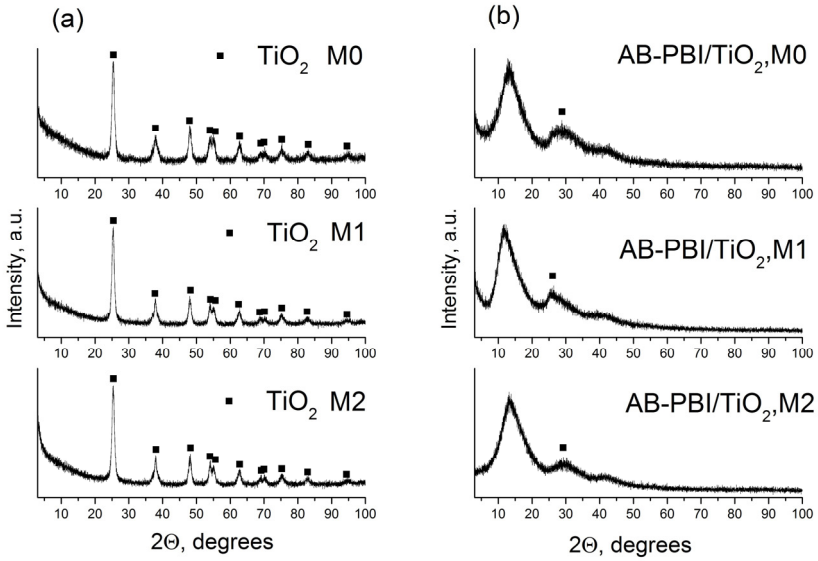


Figure 7. *Cont.*

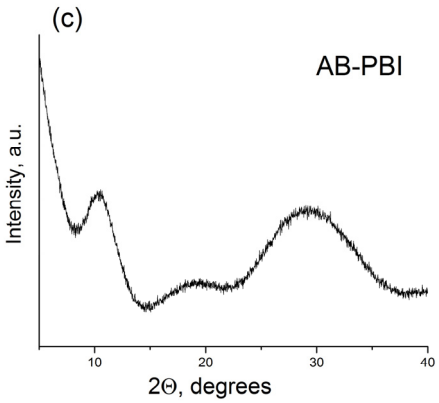


Figure 7. PXRD patterns of (**a**) green synthesized TiO_2 and (**b**) AB-PBI/bio-TiO_2 membranes and (**c**) pristine AB-PBI.

3.3.2. XPS Study

XPS was used to analyze the surface of the lyophilized membranes. Research shows that C1s, O1s, N1s, P2p, Na1s, and Ti2p peaks are registered on the surface. The atomic concentrations of the chemical elements on the surface of the membranes are represented in Table 2. The carbon spectrum is asymmetric, and shoulders toward higher binding energies are observed, which after decomposition are found to be due to C-C (285.0 eV), C-O/C=N (286.5 eV), C=O (288.3 eV), and COOH (only in the acidic form of the membrane) bonds [70]. These carbon bonds are also evidenced by the decomposed broad spectrum of oxygen, which also contains oxygen bound to phosphorus and oxygen in the water molecule. The nitrogen spectrum is associated with an imine -N=C and an amine -NH- group, with binding energies at 398.2 eV and 400 eV, respectively (Figure 8) [71]. The concentrations of up to 100% of the different C and N species are represented in Table 3. The phosphorus peak is attributed to metal phosphate with a binding energy of 133.6 eV [72], which is also proved by the Na1s peak with a binding energy of 1071.2 eV. A very small amount of titanium 0.2–0.3 at. % is also registered on the surface.

Table 2. XPS results on the surface of the AB-PBI-TiO_2, M1 membranes (neutralized and acid-doped forms).

Samples	C, at. %	O, at. %	Ti, at. %	N, at. %	P, at. %	Na, at. %
AB-PBI-TiO_2, M1 acid-doped form	57.0	26.8	0.3	9.6	5.3	1.0
AB-PBI-TiO_2, M1 neutralized form	72.4	17.1	0.2	8.3	0.8	1.2

Table 3. The percentages of C and N in various species.

Binding Energy, eV	Chemical Bonding	Concentration, %	
		AB-PBI-TiO_2, M1 Acidic Form	**AB-PBI-TiO_2, M1 Neutral Form**
285.0	C-C	61.4	76.1
286.5	C-O/C=N	26.0	14.6
288.3	C=O	9.5	9.3
289.4	COOH	3.1	-
398.2	Imine, -N=C	28.7	71.3
399.9	Amine, -NH-	27.9	72.1

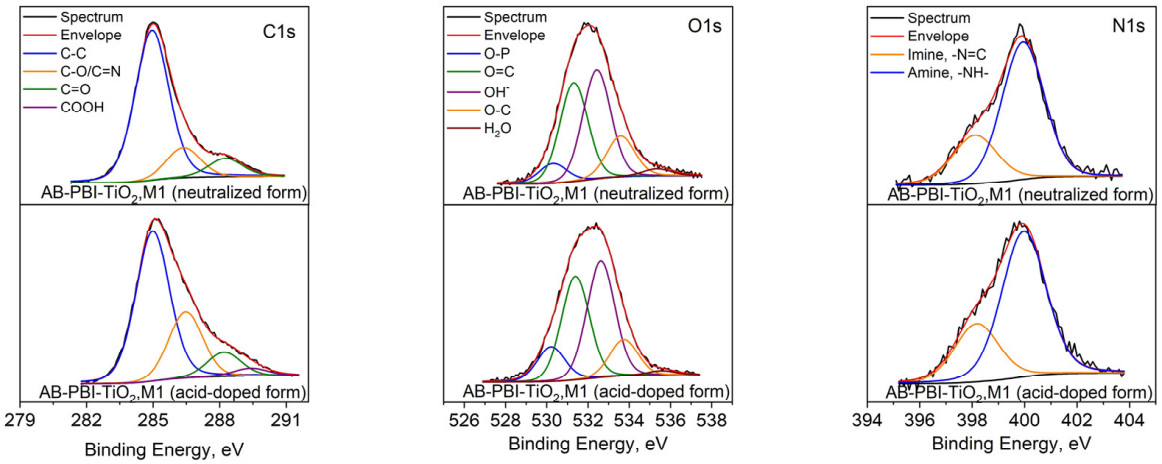


Figure 8. Deconvolution of C1s, O1s, and N1s core level spectra of the AB-PBI-TiO_2, M1 membranes (neutralized and acid-doped forms).

3.3.3. EPR Spectroscopy

EPR spectroscopy was used to characterize paramagnetic centers. In the pure polymer (polybenzimidazole PBI), an intense central signal with g_2 = 2.0025 and ΔH = 0.6 mT (peak to peak line width) is registered, along with two weakly intense satellite lines with g_1 = 1.984 and g_3 = 2.027 (Figure 9, spectrum 1). This triplet signal was previously observed in N-TiO_2 and is due to the interaction of an unpaired electron with a nuclear spin I = 1, attributed to N_b • centers formed by an unpaired 2p electron belonging to an N atom [73]. Some authors attribute this triplet to paramagnetic nitrogen oxides (such as NO, NO_2, NO_2^-, NO_2^{2-}) [74]. Additionally, a signal at g = 2.056 is registered, which could be due to adsorbed water, OH•, or absorbed oxygen O_2^-.

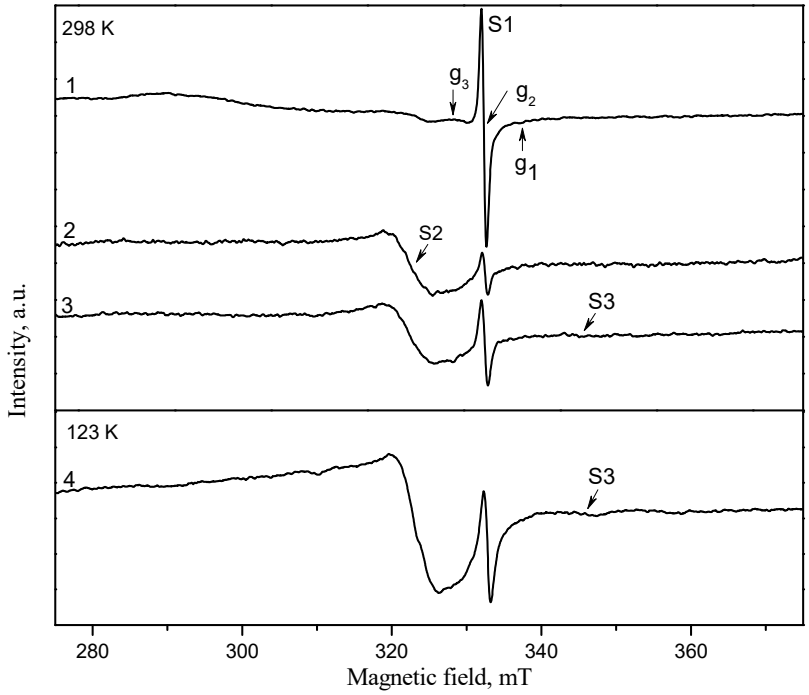


Figure 9. EPR spectra of 1—polybenzimidazole; 2—PBI/bio-TiO_2, M1 before UV irradiation; 3—PBI/bio-TiO_2, M1 after UV irradiation recorded at room temperature; 4—PBI/bio-TiO_2, M1 after UV irradiation recorded at 123 K.

The signal S1 at PBI/TiO_2 samples was less intensive than in the pure polymer. A slight shift of g-factors was observed: g_1 = 1.98, g_2 = 2.002, and g_3 = 2.015. On the other hand, a significant increase in the EPR intensity of the central peak of the triplet was observed after UV irradiation (for 40 min irradiation time, its intensity increases two times) (Figure 9, spectrum 2 and 3). As the irradiation time increases, the S1 signal intensity continues to increase. Some authors have found that bulk N_b• species are photo-dependent (photoactive), unlike NO. In our experiment, we observed an increase in signal (S1) intensity with g = 2.0025; therefore, the signal is probably due to N_b• centers particles [75]. In a study of N-doped TiO_2, some authors attributed this signal to an electron trapped in an oxygen vacancy O^- [74].

A broad asymmetric signal S2 was also recorded in the PBI/TiO_2 samples, possibly due to the overlap of two signals with close g-factors. The superimposed line recorded in the frame of 315–327 mT magnetic field may be due to adsorbed water or absorbed oxygen O_2^- [54,55] and OH• radicals adsorbed on the TiO_2 surface [53].

Ti^{3+} ions are characterized by very short relaxation time, so their EPR spectrum is better observed at low temperatures (Figure 9, spectrum 4). A broad, weakly intense line S3 appears at g = 1.93. Signals at g < 2 may be due to electrons captured by the titanium ion. The broad EPR line indicates the formation of Ti^{3+} particles at surface sites.

3.3.4. SEM and EDS Mapping/Spectra Analysis of the AB-PBI/Bio-TiO_2 Membranes

Figures 10 and 11, and Figure S1 show in-plane SEM images, and Figure S2 presents EDS spectra of the synthesized AB-PBI/bio-TiO_2, M1 (neutralized and acid-doped forms) membranes. The presence of individual and clustered micron- and submicron titania particles on the membrane surface is evidenced in both ex situ acid-doped forms and in the ammonia-neutralized membranes. The EDS spectra show mainly the presence of C, O, and Ti for both AB-PBI/bio-TiO_2, M1 (basic and acid-doped forms) membranes. The P and S contents in the AB-PBI/bio-TiO_2, M1 (acid-doped form) were due to the Eaton's reagent used (methansulfonic acid/P_2O_5) during the polycondensation process and the plant extract. The observed peaks of the other elements could be attributed to the *Mentha Spicata* plant extract used that adhered to the titania phase surface during the synthesis. The EDS results of synthesized AB-PBI/bio-TiO_2, M1 (basic and acid-doped forms) membranes, and *Mentha Spicata* plant are represented in Table 4, Tables S1 and S2. The EDS mapping analysis (Figure 11) of the prepared AB-PBI/bio-TiO_2, M1 (basic and acid-doped forms) membranes is in agreement with the conventional SEM observations, as seen from the images.

Table 4. EDS results of prepared AB-PBI/bio-TiO_2, M1 (basic form) membrane.

Element	wt. %	Atomic %
C	75.28	83.37
O	16.96	14.10
Na	0.86	0.50
Cl	1.30	0.49
K	0.80	0.27
Ti	4.04	1.12
Zn	0.76	0.15
Total	100.00	100.00

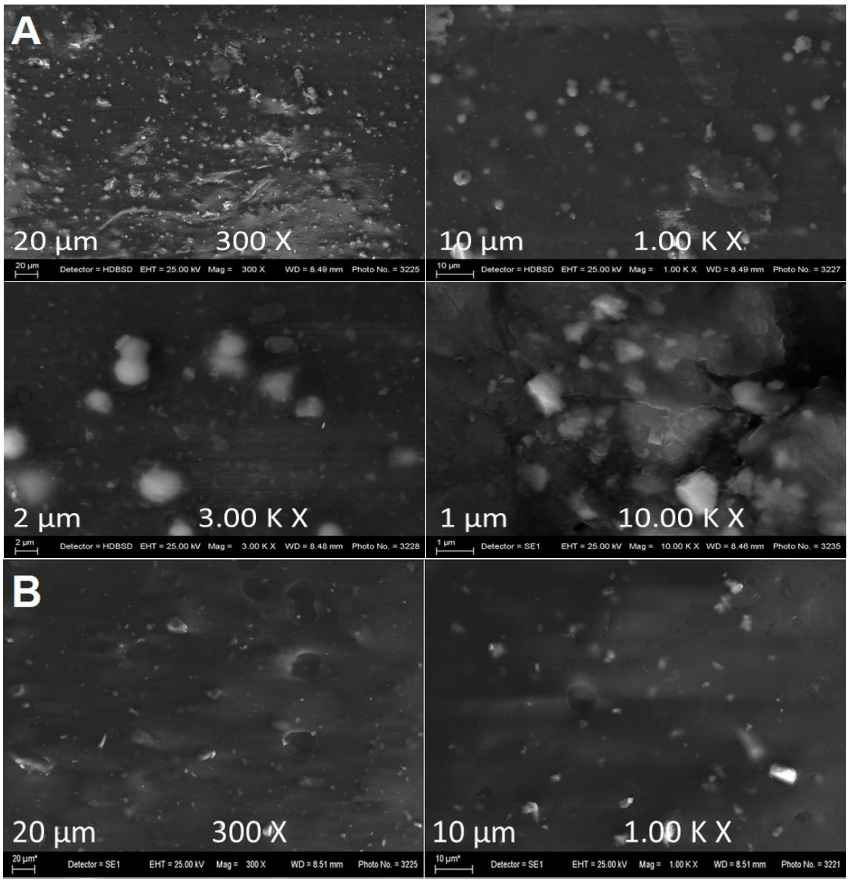


Figure 10. SEM images of (**A**) AB-PBI/bio-TiO_2, M1 (basic form) and (**B**) AB-PBI/bio-TiO_2, M1 (acid-doped form) membranes.

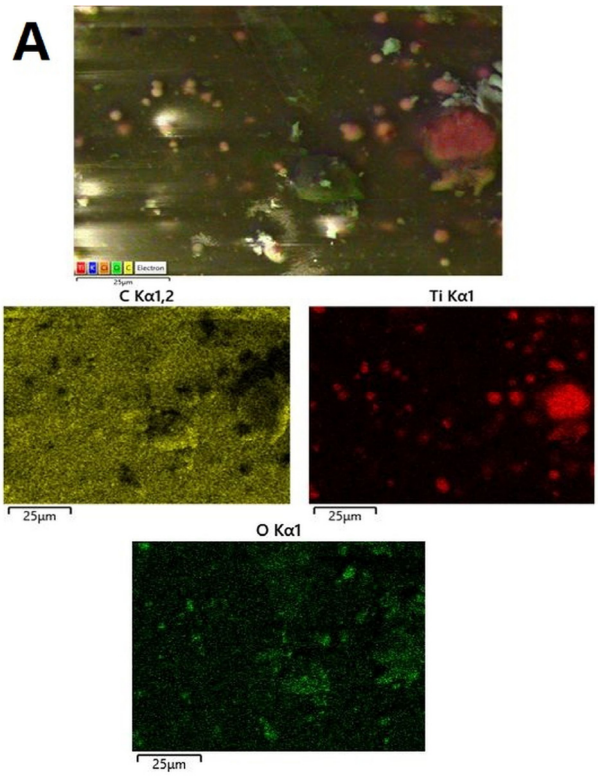


Figure 11. *Cont*.

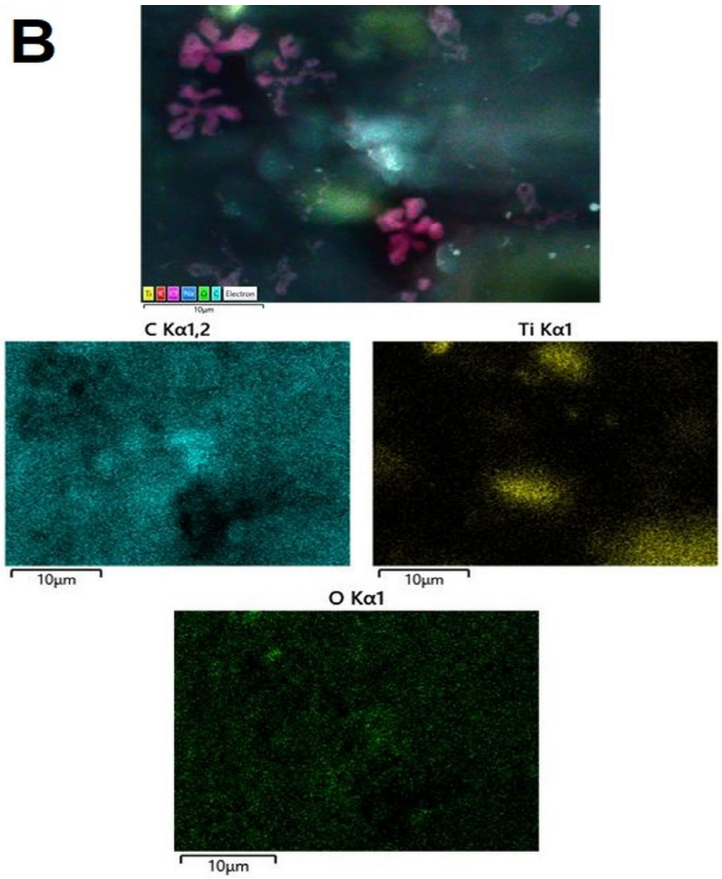


Figure 11. EDS mapping of (**A**) AB-PBI/bio-TiO_2, M1 (neutralized form) and (**B**) AB-PBI/bio-TiO_2, M1 (acid-doped form) membranes.

3.3.5. FTIR Investigations

The FTIR spectra of the green synthesized TiO_2 and AB-PBI/bio-TiO_2 membranes are shown in Figure 12. In the FTIR spectra of green synthesized TiO_2, one can observe a broad band around 3389 cm^{-1} corresponding to the stretching vibration of the O–H bond. The peak at 1633 cm^{-1} is attributed to the O–H bending vibration of adsorbed water molecules on the surface of synthesized TiO_2. The peaks within the region 443 cm^{-1}–453 cm^{-1} are associated with the Ti–O bending vibration, characteristic of the formation of metal–oxygen bonding [76,77]. The pristine AB-PBI represents some characteristic absorption bands at 1602, 1547, and 1286 cm^{-1} arising from the C–N stretching, –N–H stretching, and from the bending mode of the imidazole ring, respectively [78].

The appearance of new bands at 2920 and 2894 cm^{-1} in the FTIR spectrum of AB-PBI/TiO_2, M2 due to the C–H stretching mode confirms the presence of organic guest moieties. Some common bands that were also present in the pure AB-PBI and AB-PBI/TiO_2, M1 membrane showed the insertion of TiO_2 in the polymer matrix without changing its chemical structure.

With the inclusion of TiO_2 in the composite membranes, the peak attributed to the N-H stretching broadens to a wider range of 3400–2920 cm^{-1}. This is due to the presence of an H-bond in the PBI repeating unit and the TiO_2 particles. This is also an indication of a good distribution of TiO_2 inside the polymer matrix.

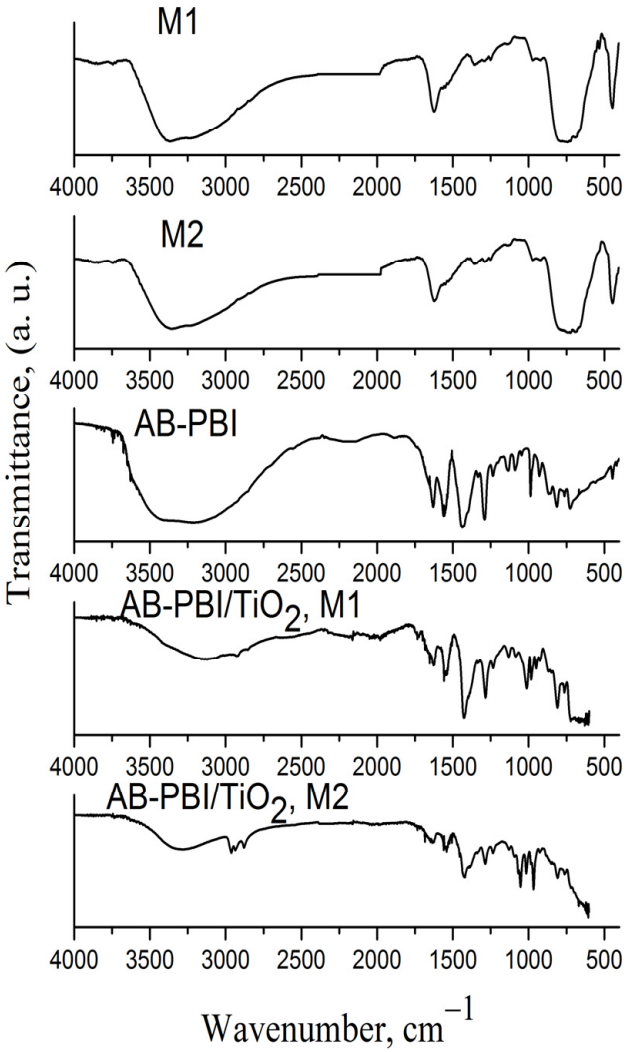


Figure 12. FTIR spectra of green synthesized TiO_2 and AB-PBI/bio-TiO_2 membranes.

3.3.6. Thermogravimetric Analysis (TG) of the Prepared AB-PBI/Bio-TiO_2 Membranes

TG curves of lyophilized pristine AB-PBI and different AB-PBI/bio-TiO_2 composite membranes (Figure 13) revealed the characteristic high chemical decolorization temperature of AB-PBI starting above 650 °C. Initial loss of up to ~300 °C is attributed to the free moisture and the loss of the imidazole H-bonded water molecules, as observed with other aromatic polybenzimidazoles [79]. The closely packed macromolecular structure of AB-PBI compared with the much loosely-packed meta- and para-PBIs is responsible for the sluggish release of water due to stronger high-density imidazole H-bonding—NH group density, defined as the percent of molar mass of N–H group per repeat unit = 12.9%, compared to m-PBI (NH group density = 9.7%) [80]. Similar moisture loss was noted for both analyzed composite samples with incorporated plant extract synthesized titania particles with a higher degree of crystallinity (samples M1 and M2). The char yields at 800 °C of both M1 and M2 titania composite samples (30 and 35% resp.) were found to be much lower than those of the pristine AB-PBI (45%). This is an indication of the efficient incorporation of nanocrystalline TiO_2 particles within the AB-PBI matrix, as the titania anatase phase is thermooxidation stable even at this relatively high polymer carbonization temperature.

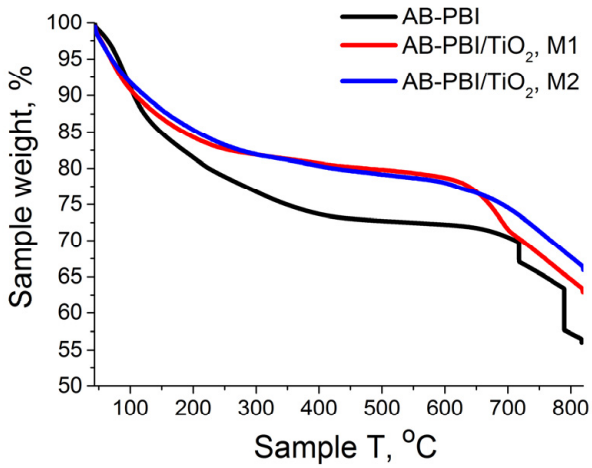


Figure 13. Thermogravimetric curves of AB-PBI/TiO_2 membranes.

3.4. Photocatalytic Study of Prepared AB-PBI/Bio-TiO_2 Membranes

The photocatalytic activity of the prepared AB-PBI/bio-TiO_2 membranes has been studied in the reaction of the photocatalytic decolorization of Reactive Black 5 dye as a model pollutant in aqueous solutions (Figures 14–16). In the presence of AB-PBI/bio-TiO_2, M1 and M2 (neutralized and acid-doped forms), the photocatalytic decolorization of RB5 dye proceeds in two stages (0–60 min and 90–180 min), while in the case of AB-PBI/bio-TiO_2, M0 (basic and acid-doped forms), it is in one stage (0–180 min). The values of the calculated apparent rate constants are AB-PBI/bio-TiO_2, M1 (basic form) > AB-PBI/bio-TiO_2, M1(acid-doped form); AB-PBI/bio-TiO_2, M2 (basic form); AB-PBI/bio-TiO_2, M2 (acid-doped form); AB-PBI/bio-TiO_2, M0 (basic form); AB-PBI/bio-TiO_2, M0 (acid-doped form) for 180 min under UV irradiation. The basic forms of all investigated AB-PBI/bio-TiO_2 membranes demonstrated higher photocatalytic ability compared to the acidic forms. The highest degree of decolorization of the model dye was achieved in the presence of photocatalyst membranes AB-PBI/bio-TiO_2, M1 (96% and 89% for the basic and acid forms, respectively). Composites M2 show slightly lower decolorization values, 88% and 56%, for the neutralized and acid-doped forms, respectively. Membranes containing MO particles have the lowest value of photocatalytic decolorization, 57% and 58% for the basic and acid-doped forms, respectively. Table 5 gives the results presented in the literature about the removal of organic pollutants using hybrid photocatalysts.

It is well known that the presence of point defects and oxygen vacancies in the TiO_2 lattice influences many surface reactions. Among them, Ti^{3+} ions are significant reactive agents for many adsorption processes. They can induce the formation of oxygen vacancies [87]. It was proved that both Ti^{3+} and oxygen vacancies have a synergistic effect on the rate of the photocatalytic reactions due to their possibility to separate the light-induced electron–hole pairs (thanks to the formation of sub-levels in the conduction band of TiO_2) and increase its redox capacity [88]. The samples AB-PBI/bio-TiO_2, M1 exhibit the highest photocatalytic reaction rate towards the azo dye as a result of the optimal combination of the presence of Ti^{3+} defects, oxygen vacancies, crystallites sizes, degree of crystallinity, decreased band gap value, and homogeneous distribution of the nanocrystallites (proved by TEM, XRD, XPS, and EPR analyses). The presence of aggregates composed of particles having different sizes in M2 samples negatively influences their photocatalytic activity by the following physicochemical effects: (i) decreased light intensity reaching the surface, thus resulting in a reduced quantum yield; (ii) less active sites, available for the dye adsorption on the surface of the membrane. These above-mentioned effects could be responsible for the slower decolorization rate of the dye in the presence of AB-PBI/bio-TiO_2, M2 composites.

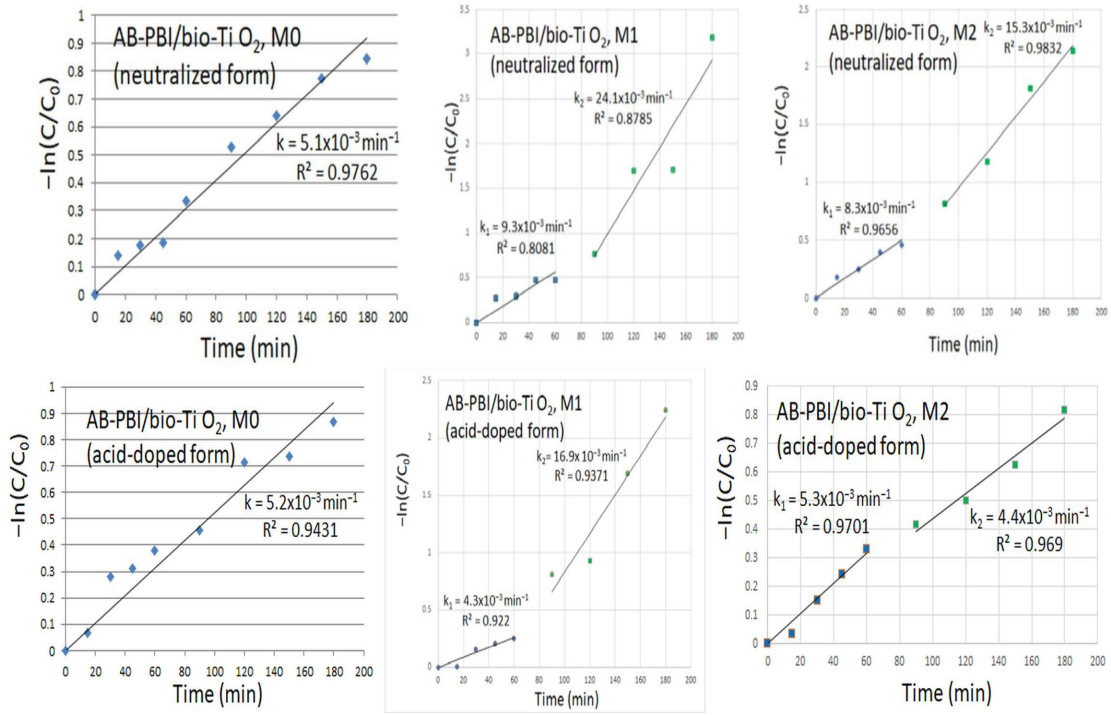


Figure 14. Kinetic curves of UV decolorization of Reactive Black 5 dye using AB-PBI/bio-TiO_2 membranes as photocatalysts.

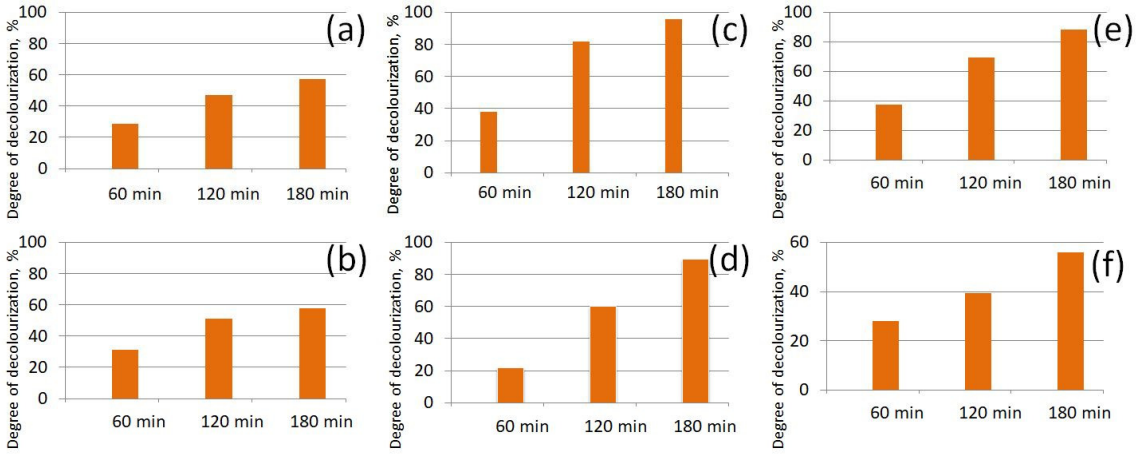


Figure 15. Degree of decolorization of RB 5 dye during UV irradiation time period using (**a**,**b**) AB-PBI/bio-TiO_2, M0 (neutralized and acid-doped forms); (**c**,**d**) AB-PBI/bio-TiO_2, M1 (neutralized and acid-doped forms); (**e**,**f**) AB-PBI/bio-TiO_2, M2 (neutralized and acid-doped forms) membranes as photocatalysts.

The following mechanism of photocatalytic reaction could be proposed: There are probably three mechanisms occurring simultaneously. (1) Direct oxidation of pollutant molecules on the surface of the TiO_2 particles–electron transfer to positively charges holes in the valence band-heterogeneous catalysis. (2) In homogeneous catalysis, there are two mechanisms of indirect oxidation: the interaction of pollutant molecules with hydroxyl radicals (a radical-chain mechanism) and their interaction with oxygen radical anions. Figure 15 shows the degree of decolorization of RB5 dye during the UV irradiation time period using AB-PBI/bio-TiO_2 membranes (neutralized and acid-doped forms) as photocatalysts. Figure 16 represents UV–Vis absorption spectra of RB5 dye during the irradiation time period using AB-PBI/bio-TiO_2, M1 (basic form) as the photocatalyst.

Figure 17 presents the adsorption capacities of AB-PBI/bio-TiO_2, M0, M1, and M2 (neutralized and acid-doped forms) membranes after a 30 min dark period. The highest adsorption capacity is demonstrated by AB-PBI/bio-TiO_2, M2 (acid-doped form). The lowest adsorption capacity is demonstrated by AB-PBI/bio-TiO_2, M0 (neutralized form). The adsorption capacities of AB-PBI/bio-TiO_2, M1 and M2 (neutralized forms) are equal. In the available current literature, the data about the influence of the adsorption ability on the photocatalytic efficiency are quite contradictory. In our case, the higher adsorption abilities of all the types of membrane contact do not lead to any enhancement of the photocatalytic characteristics. It can be concluded that the photocatalytic reaction rate does not depend on the adsorption capacity of the AB-PBI/bio-TiO_2 membranes.

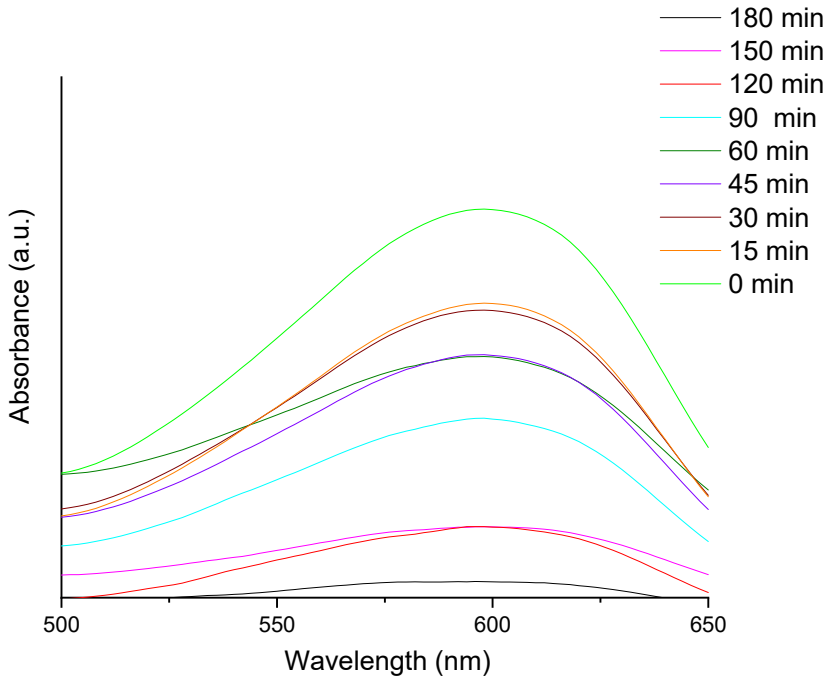


Figure 16. UV–Vis absorption spectra of RB 5 dye during irradiation time period using AB-PBI/bio-TiO_2, M1 (basic form) as the photocatalyst.

Table 5. The removal of organic pollutants using hybrid photocatalysts by literature data.

Materials	Processes	Type of Pollutant Removed	Lamp Source	Removal Efficiency	References
PVDF@TiO_2	blending, dip coating, and grafting	Methylene blue dye	UV light	95.4%	[81]
PVA /TiO_2	electrospinning	Rhodamine B dye	Vis light	80%	[82]
PANI-TiO_2	template free method	Reactive Black 5 dye	Vis light	96%	[83]
PPy-TiO_2	chemical oxidative polymerization method	Methylene blue dye	Solar light	93%	[84]
PVDF/TiO_2	phase inversion Method	brilliant green dye	UV light	~45%	[85]
TiO_2/PFT	surface modification	phenol	Vis light	74.3%	[86]

The investigated AB-PBI/bio-TiO_2 photocatalysts preserved their photocatalytic ability relatively well after three photocatalytic runs, which, in fact, demonstrates their suitable long-term stability (Figure 18). As can be seen, the degree of RB 5 dye decolorization decreased very slightly, starting from the first until the third cycle.

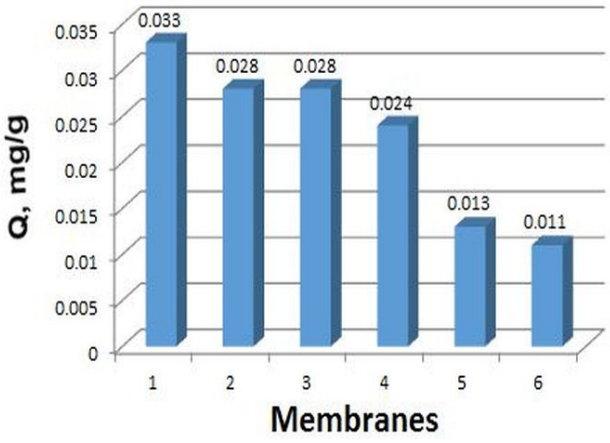


Figure 17. The adsorption capacities (Q) (mg/g) of (1) and (2) AB-PBI/bio-TiO_2, M2 (acid-doped and neutralized forms); (3) and (4) AB-PBI/bio-TiO_2, M1 (neutralized and acid-doped forms); (5) and (6) AB-PBI/bio-TiO_2, M0 (acid-doped and neutralized forms) membranes after a 30 min dark period.

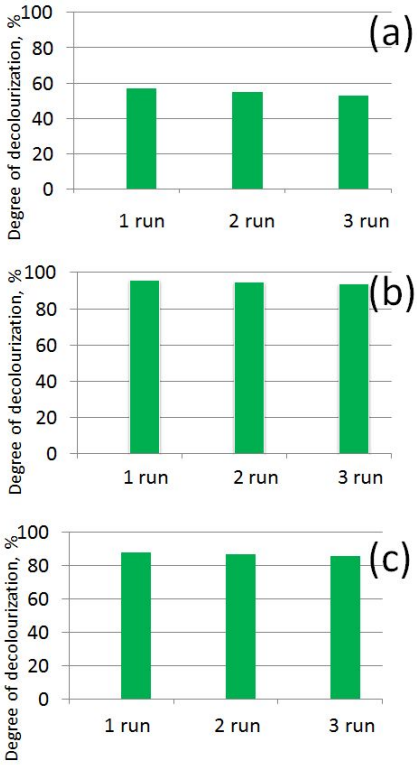


Figure 18. Degree of decolorization of RB 5 dye after 180 min under UV irradiation using basic form membranes in three photocatalytic runs. (**a**) AB-PBI/bio-TiO_2, M0; (**b**) AB-PBI/bio-TiO_2, M1; and (**c**) AB-PBI/bio-TiO_2, M2.

3.5. Antibacterial Activity of Prepared AB-PBI/Bio-TiO_2 Membranes

The quantitative RMDA method, applied by us, showed that the TiO_2 nanopowders had no antimicrobial activity at the tested concentrations (5, 20 mg/mL), both under static and dynamic conditions. In comparison, Chakansin et al. (2022) [89] report resazurin bleaching at approximately > 50 mg/mL of TiO_2. The thorough review of Serov et al. (2024) [44], which uses the data from tens of publications, points out TiO_2 NPs MICs range from 0 to approx 2500 μg/mL.

The data on TiO_2 NP antimicrobial activity not only vary widely in MIC values, but they are contradictory in view of the requirement for visible or UV light irradiation. Some authors report the antimicrobial activity of TiO_2 in the dark [90–92]. According to other

authors, the antimicrobial application of TiO_2 requires illumination in the visible or the UV spectrum [40,41,93,94]. Our experiments also show definite antimicrobial activity of titanium dioxide nanoparticles only under UV light irradiation. This has been demonstrated by the parallel testing of a bacterial suspension containing 0.5 mg/mL of each TiO_2 nanopowder and the same suspension irradiated by UV light. Both suspensions were under continuous stirring to avoid particle sedimentation. The results for M0, M1, and M2 showed a significant reduction in CFU as early as the 10th minute of exposure by three exponents and a further reduction of up to four exponents at the 20th minute. Another interesting result was observed for M1 and M2: at the 30th minute of irradiation, the number of registered living cells was greater than that at the 10th and 20th minutes but still remained significantly lower (by two to three exponents) than that of the non-irradiated suspension (Figure 19). The same phenomenon was described by Sirelkhatim et al. (2015) [45]. A slight enhancement of the antibacterial effect was observed in the sequence M0 < M1 < M2, which coincides with the increase of the $O_{total}/O_{lattice}$ ratio of the nanoparticles.

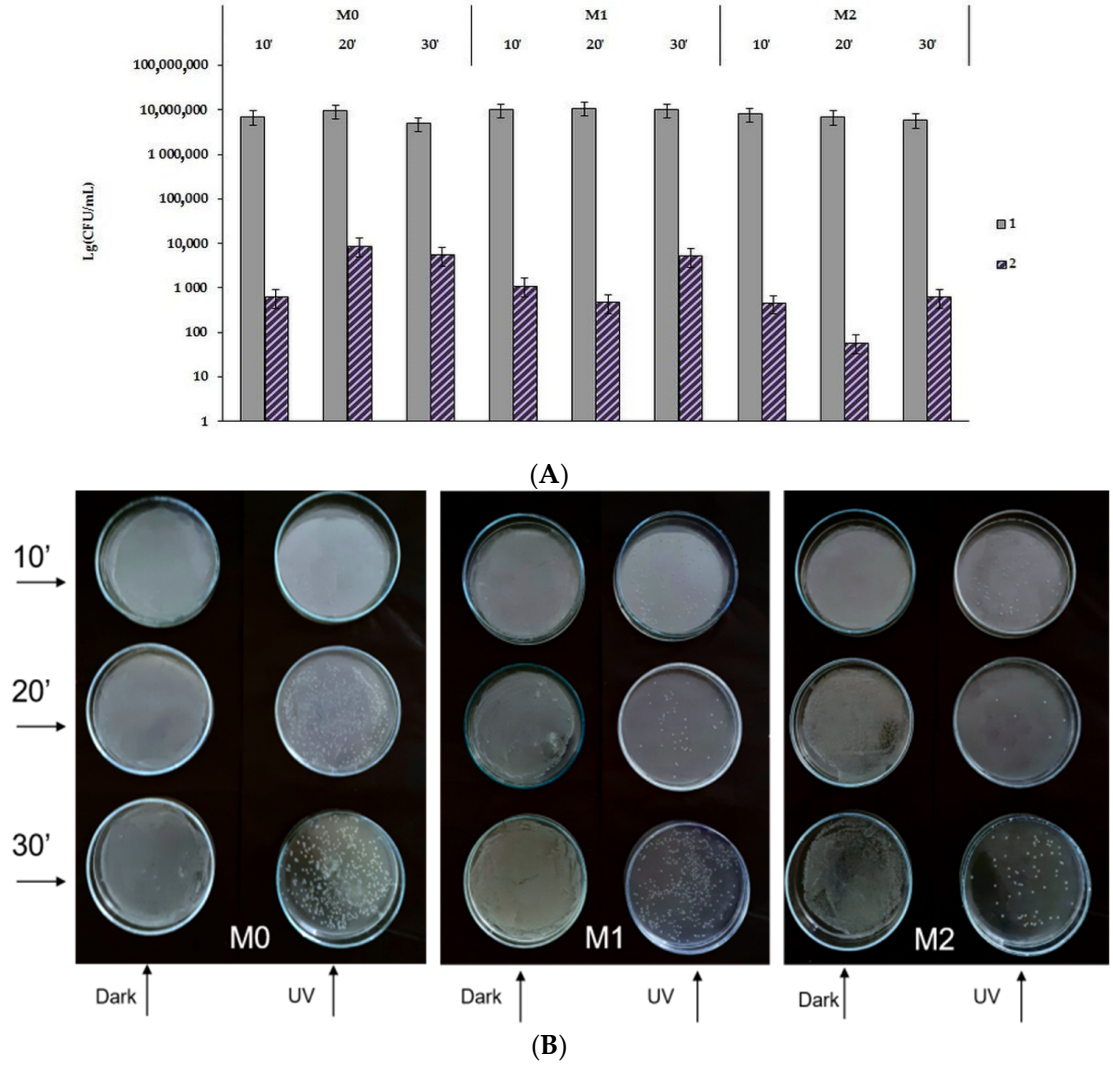


Figure 19. (**A**) Antimicrobial effect of the UV-irradiated (violet columns) suspensions of M0, M1, and M2 (0.5 mg/mL) with *E. coli* compared with their equivalents kept in the dark (gray columns) expressed as CFU/mL. (**B**) The decrease of CFU under UV light is well visible in the petri dishes.

In order to determine whether the composite materials have antimicrobial activity in the dark, we applied the ASTM method, which is aimed at testing the antimicrobial properties of polymer materials in dynamic contact with bacterial suspension. Similar to

the results from the RMDA procedure, this method showed no antimicrobial activity of the composite membranes in the dark. A slight stimulatory effect of the materials towards bacterial cells was even observed, which is probably due to the properties of the PBI carrier membrane (Figure 20).

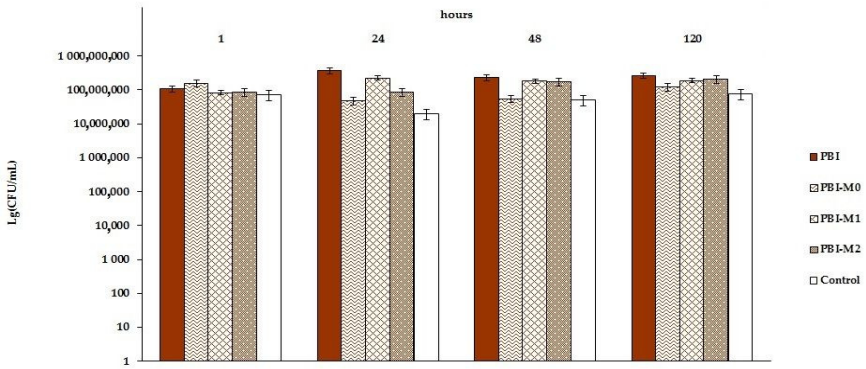


Figure 20. Antimicrobial effect of the composite membranes AB-PBI/bio-TiO_2, M0, AB-PBI/bio-TiO_2, M1, and AB-PBI/bio-TiO_2, M2 on *E. coli* in the dark tested by the ASTM Standard Test Method E 2149–10. Control samples contain only bacterial suspension.

The antimicrobial properties of the composite membranes were clearly manifested after irradiation by UV light (Figure 21). All three composites showed very good antimicrobial activity, with CFU counts decreasing by two to three logarithms after 10 min of irradiation. The presence of TiO_2 NPs in the membranes enhances the effect of UV light, and it leads to a stronger reduction in CFU compared to the control sample, which contains only bacterial cells and it also shows some reduction in CFU due to the UV light. The AB-PBI/bio-TiO_2, M1 material showed the best antimicrobial effect.

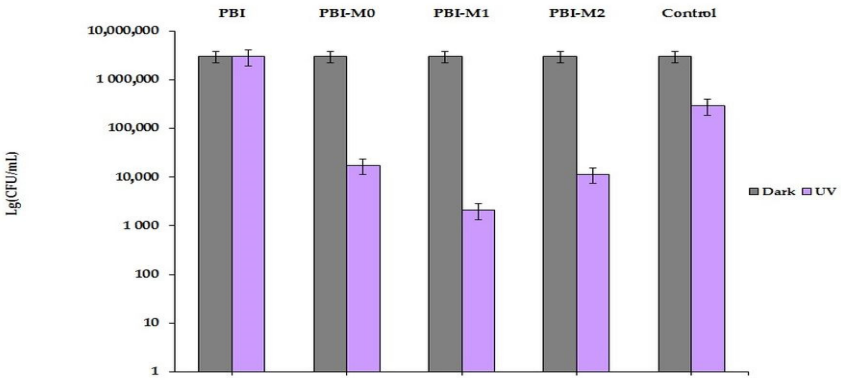


Figure 21. Effect of AB-PBI-TiO_2 composites on standard *E. coli* suspension under UV irradiation for 10 min. Control samples contain only bacterial suspension.

Remarkably, the test samples of pristine AB-PBI membrane in neutral form did not show a decrease in cell number upon UV-light irradiation (Figure 21). As it was expected, the control samples containing only bacterial suspension showed a decrease in the number of cells as a result of the UV-irradiation by approx. one logarithm. It is likely that pure AB-PBI membrane possesses distinguished UV-photosensitization properties, which partially neutralize the bactericidal effects of UV radiation. Taking into account the well-known common sunscreen low-molecular constituent, 2-phenylbenzimidazole-5-sulfonic acid (PBSA), this hypothesis is highly likely. In a previous experiment, which aimed to test the effect of the combination of cellulose membrane surface impregnated with meta-PBI, we observed an increase in the number of viable *E. coli* and *B. subtilis* cells over 120 h [52]. To the best of our knowledge, such an experiment using AB-PBI membrane is conducted for the first time, and the data obtained from it, are pristine for further investigation. In the

scientific literature available to us, we could not find any studies of the effect of any PBIs on microbial culture growth or inhibition. Further experiments are needed to investigate these interesting features.

Bacterial morphology assessment by SEM

After UV irradiation, during cultivation on composite membranes AB-PBI/bio-TiO_2, M0, swellings on the cell surface were observed (indicated by white arrows). We observed similar structural changes in our previous studies on Pseudomonas aeruginosa biofilms treated using cationic polymer micelles loaded with silver nanoparticles [36]. Moreover, in the represented micrograph of this double-treated sample, a certain destructive effect on the bacterial cells is evident. Localized damage appears on the bacterial cell wall, likely affecting the underlying membranes, resulting in rupture and separation of cell contents (indicated by white triangles) (Figure 22a).

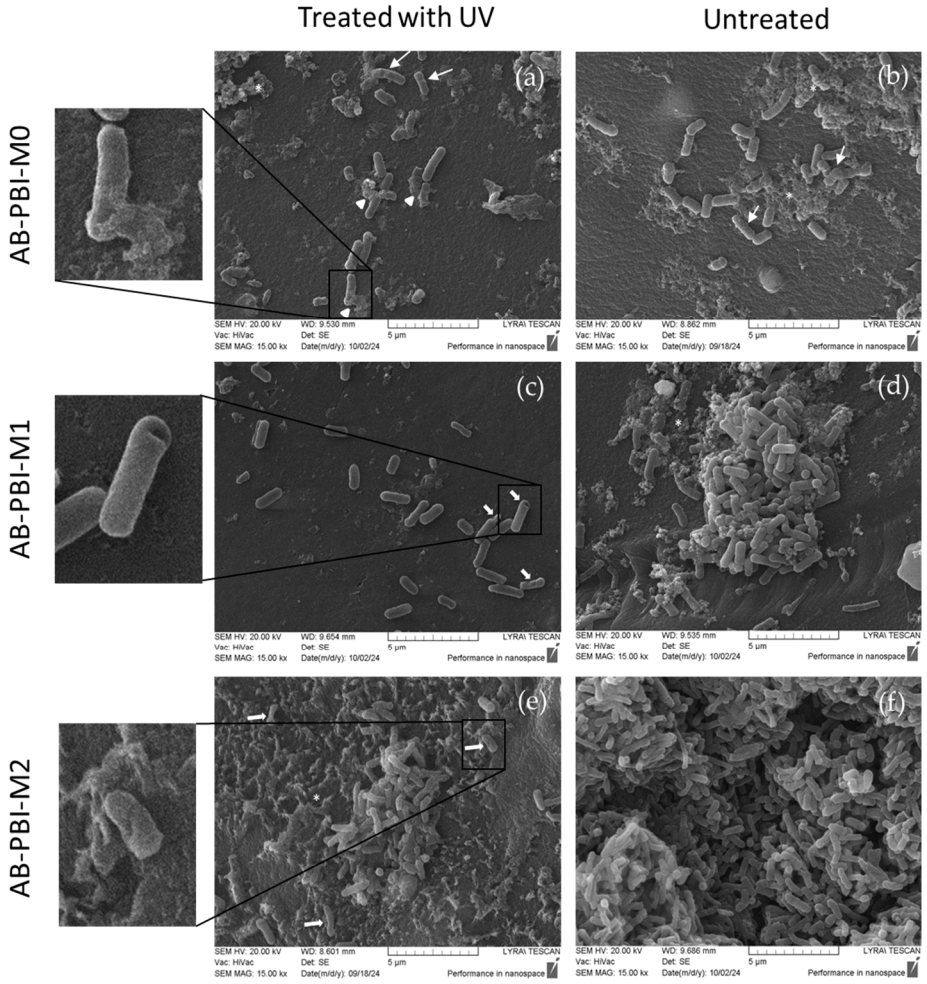


Figure 22. Representative SEM micrographs revealing the surface morphology and adhesion of *E. coli* 25922 during cultivation with composite membranes AB-PBI/bio-TiO_2, M0 ((**a**)—treated with UV, 10 min. (**b**)—untreated), AB-PBI/bio-TiO_2, M1 ((**c**)—treated with UV, 10 min. (**d**)—untreated) and AB-PBI/bio-TiO_2, M2 ((**e**)—treated with UV, 10 min, (**f**)—untreated). Designations: White arrows—blebs or invaginations; white triangle—ruptured cells; white stars—amorphous substance. Zoom images highlight some of the damage in the bacterial cells. Bars = 5 µm.

It is important to note that for normal cellular function, the permeability of the bacterial cell wall and membranes is vital due to their protective role in oxidative phosphorylation mechanisms. In contrast, in the untreated sample, the bacterial cell morphology was relatively preserved, except for the appearance of swellings in localized areas of the cell

wall. A residual amorphous substance was also prevalent around or on the bacterial cells (indicated by white stars) (Figure 22b). In all the double-treated samples, following UV activation of TiO_2 nanoparticles, shortened cells were observed, a finding not visible in the case of unirradiated samples (Figure 22a,c,e). This heterogeneity in the bacterial population is probably due to the combined effects of UV irradiation and the concentration of added TiO_2 nanoparticles. These factors likely delayed cell growth and they altered the physiological activity of the cells, as it is confirmed by the antibacterial effect analysis (Figures 20 and 21). Additionally, a reduction in the number of adhered bacterial cells was reported in all three treated samples (Figure 22b,d,f) compared to the untreated ones. In the non-irradiated sample AB-PBI/bio-TiO_2, M2, the localization of the cells resembled biofilm consortia with a ubiquitous, multilayered architecture (Figure 22). Suppression of bacterial adhesiveness is a key mechanism in preventing the spreading and colonization of new niches by pathogenic bacteria, which are associated with infectious and biofilm diseases [95]. The accumulated amorphous substance likely contains TiO_2 nanoparticles, which, in samples AB-PBI/bio-TiO_2, M0 and AB-PBI/bio-TiO_2, M1, surround some of the bacterial cells (Figure 22a,b,d). In sample M2, this substance is primarily concentrated in the underlying substrate, forming small island-like protrusions (Figure 22e). Both in AB-PBI/bio-TiO_2, M1 and in AB-PBI/bio-TiO_2, M2 samples, bacterial cells with atypical shapes and disorganization in the cell wall manifested as indentations (indicated by white arrows) were observed, suggesting a destructive effect resulting from the treatment (Figure 22c,e). We assume that the damage to the cell structure is probably due to the presence of reactive oxygen species (ROS) generated by the irradiation of TiO_2 nanoparticles embedded in the membranes, as confirmed by other researchers [46,96,97].

4. Conclusions

A series of novel AB-Polybenzimidazole/green synthesized TiO_2 (20 wt.%) membranes (in basic and acidic form) were successfully prepared. It established the optimal MS extract quantity for the synthesis of TiO_2 particles for incorporation in AB-PBI membranes having high photocatalytic and antimicrobial activity. It has to be noted the key role of the plant extract for the decrease of the band gap value, defective lattice structure, and distribution of the obtained titania particles. Both EPR and XPS analyses proved that both the Ti^{3+} and oxygen vacancies in the lattice increase with the increase of the extract quantity. By means of TEM, studies have revealed that the MS leaf extract plays a stabilizing and capping role, preventing the aggregation of the particles. We evaluated the optimal plant extract quantity, leading to a homogeneous distribution of the particles.

The AB-PBI/bio-TiO_2 membranes possess high photocatalytic activity towards the decolorization of RB 5 dye under UV light irradiation (96% and 89% for neutralized and acid-doped forms, respectively)). All basic membranes exhibit long-term stability under three consecutive photocatalytic cycles. The newly synthesized AB-PBI/bio-TiO_2 membranes have a powerful antibacterial effect on *E. coli* when irradiated by UV light. The presence of TiO_2 NPs in the membranes enhances the effect of UV light and it leads to a stronger reduction in CFU compared to the control sample. The combined effects of UV irradiation and the TiO_2 particle concentration likely delayed cell growth and altered the physiological activity of the cells.

Supplementary Materials: The following supporting information can be downloaded at: https://www.mdpi.com/article/10.3390/cryst14121081/s1, Figure S1: SEM images of AB-PBI/bio-TiO_2, M1 (acid-doped form) membranes; Figure S2: EDS spectra of (A) AB-PBI/bio-TiO_2, M1 (neutralized form), (B) AB-PBI/bio-TiO_2, M1 (acid-doped form) membranes and (C) *Mentha Spicata* plant; Table S1: EDS results of prepared AB-PBI/bio-TiO_2, M1 (acid-doped form) membrane; Table S2: EDS results of *Mentha Spicata* plant.

Author Contributions: Conceptualization, H.P., I.S., K.Z. and R.E.; methodology, H.P., K.Z., I.S., D.S. and R.E. and validation, K.Z., H.P., R.E. and I.S.; formal analysis, M.S., R.M., O.D., S.D., T.P.-K., I.L. and S.E.; investigation, K.Z., H.P., I.S., D.S., M.S., R.M., I.T., R.E., I.L., T.P.-K., S.E. and R.M.;

resources, H.P., K.Z. and I.S.; data curation, K.Z., H.P., I.S., R.M., M.S. and R.E.; writing—original draft preparation, K.Z., H.P., I.S., D.S., M.S., R.M. and R.E.; writing—review and editing, K.Z., H.P., I.S., R.E. and D.S.; visualization, K.Z. and H.P.; supervision, H.P., K.Z. and I.S.; project administration, H.P., K.Z. and I.S.; funding acquisition, H.P., K.Z. and I.S. All authors have read and agreed to the published version of the manuscript.

Funding: This research was funded by the Bulgarian National Science Fund, Grant number KP-06-N69/8.

Data Availability Statement: Data are included in the manuscript.

Acknowledgments: The authors express their gratitude to the project with the Bulgarian National Science Fund, KP-06-N69/8 (КП-06-Н69/8), "Novel polymer-hybrid materials containing (bio)synthesized metal oxide particles pwith improved photocatalytic and antimicrobial potential" for the financial support. Research equipment of "Energy storage and hydrogen energetics (ESHER)", part of the Bulgarian National Roadmap for Research Infrastructure 2017–2023, approved by DCM No 354/29.08.2017 under Grant Agreement DO1-349/13.12.2023, was used in this investigation. The authors acknowledge the technical support from the project PERIMED BG05M2OP001-1.002-0005/29.03.2018 (2018–2023). We thank to A. Eliyas from Institute of Catalysis, Bulgarian Academy of Sciences for the useful discussion and to F. Ublekov from IP-BAS for the kind support.

Conflicts of Interest: The authors declare no conflicts of interest.

References

1. Honma, I.; Nomura, S.; Nakajima, H. Protonic conducting organic/inorganic nanocomposites for polymerelectrolyte membrane. *J. Membr. Sci.* **2001**, *185*, 83–94. [CrossRef]
2. Sengodu, P.; Deshmukh, A. Conducting polymers and its Inorganic composites for Advanced Li ion Batteries: A review. *RSC Advances* **2012**, *1–3*, 1–23. [CrossRef]
3. Morales-Acevedo, A. (Ed.) *Solar Cells-Research and Application Perspectives*; InTech: Rijeka, Croatia, 2013; 386p, ISBN 978-953-51-1003-3.
4. Laberty-Robert, C.; Vallé, K.; Pereira, F.; Sanchez, C. Design and properties of functional hybrid organic-inorganic membranes for fuel cells. *Chem. Soc. Rev.* **2011**, *40*, 961–1005. [CrossRef] [PubMed]
5. Liras, M.; Barawi, M.; de la Peña O'Shea, V.A. Hybrid materials based on conjugated polymers and inorganicsemiconductors as photocatalysts: From environmental to energy applications. *Chem. Soc. Rev.* **2019**, *48*, 5454–5487. [CrossRef] [PubMed]
6. Raghunath, A.; Perumal, E. Metal oxide nanoparticles as antimicrobial agents: A promise for the future. *Int. J. Antimicrob. Agents* **2017**, *49*, 137–152. [CrossRef]
7. Zare, M.; Namratha, K.; Thakur, M.S.; Byrappa, K. Biocompatibility assessment and photocatalytic activity of bio-hydrothermal synthesis of ZnO nanoparticles by Thymus vulgaris leaf extract. *Mater. Res. Bull.* **2019**, *109*, 49–59. [CrossRef]
8. Alamdari, S.; Ghamsari, M.S.; Lee, C.; Han, W.; Park, H.-H.; Tafreshi, M.J.; Afarideh, H.; Majles Ara, M.H. Preparation and Characterization of Zinc Oxide Nanoparticles Using Leaf Extract of Sambucus ebulus. *Appl. Sci.* **2020**, *10*, 3620. [CrossRef]
9. Kumar, B.; Smita, K.; Cumbal, L.; Debut, A. Green Approach for Fabrication and Applications of Zinc Oxide Nanoparticles. *Bioinorg. Chem. Appl.* **2014**, *2014*, 523869. [CrossRef]
10. Punnoose, A.; Dodge, K.; Rassmussen, J.; Chess, J.; Wingett, D.; Ander, C. Cytotoxicity of ZnO nanoparticles can be tailored by modifying their surface structure: A green chemistry approach for safer nanomaterials. *ACS Sustain. Chem. Eng.* **2014**, *2*, 1666–1673. [CrossRef]
11. Verma, V.; Al-Dossari, M.; Singh, J.; Rawat, M.; Kordy, M.G.M.; Shaban, M. A Review on Green Synthesis of TiO_2 NPs: Photocatalysis and Antimicrobial Applications. *Polymers* **2022**, *14*, 1444. [CrossRef]
12. Muniandy, S.S.; NH Mohd, K.; Jiang, Z.T.; Altarawneh, M.; Lee, H.L. Green synthesis of mesoporous anataseTiO_2 nanoparticles and their photocatalytic activities. *RSC Adv.* **2017**, *7*, 48083–48094. [CrossRef]
13. Sundrarajan, M.; Bama, K.; Bhavani, M.; Jegatheeswaran, S.; Sumathi, R. Obtaining titanium dioxide nanoparticles with spherical shape and antimicrobial properties using M. citrifolia leaves extract by hydrothermal method. *J. Photochem. Photobiol. B Biol.* **2017**, *171*, 117–124. [CrossRef]
14. Zyoud, S.H.; Ganesh, V.; Che Abdullah, C.A.; Yahia, I.S.; Zyoud, A.H.; Abdelkader, A.F.I.; Daher, M.G.; Nasor, M.; Shahwan, M.; Zahran, H.Y.; et al. Facile Synthesis of Ni-Doped ZnO Nanostructures via Laser-Assisted Chemical Bath Synthesis with High and Durable Photocatalytic Activity. *Crystals* **2023**, *13*, 1087. [CrossRef]
15. Li, S.; Dong, K.; Cai, M.; Li, X.; Chen, X. A plasmonic S-scheme Au/MIL-101(Fe)/BiOBr photocatalyst for efficient synchronous decontamination of Cr(VI) and norfloxacin antibiotic. *eScience* **2024**, *4*, 100208. [CrossRef]
16. Rajesh, D.; Ahuja, T.; Kumar, D. Recent progress in the development of nano-structured conducting polymers/nanocomposites for sensor applications. *Sens. Actuators B* **2009**, *136*, 275–286. [CrossRef]
17. Leong, S.; Razmjou, A.; Wang, K.; Hapgood, K.; Zhang, X.; Wang, H. TiO_2 based photocatalytic membranes: A review. *J. Membr. Sci.* **2014**, *472*, 167–184. [CrossRef]

18. Kleine, J.; Peinemann, K.V.; Schuster, C.; Warnecke, H.J. Multifunctional system for treatment of wastewaters from adhesive-producing industries: Separation of solids and oxidation of dissolved pollutants using doted microfiltration membranes. *Chem. Eng. Sci.* **2002**, *57*, 1661–1664. [CrossRef]
19. Rahimpour, A.; Jahanshahi, M.; Rajaeian, B.; Rahimnejad, M. TiO_2 entrapped nano-composite PVDF/SPES membranes: Preparation, characterization, anti fouling and antibacterial properties. *Desalination* **2011**, *278*, 343–353. [CrossRef]
20. Kim, S.H.; Kwak, S.-Y.; Sohn, B.-H.; Park, T.H. Design of TiO_2 nanoparticle self assembled aromatic polyamide thin-film-composite (TFC) membrane as an approach to solve biofouling problem. *J. Membr. Sci.* **2003**, *211*, 157–165. [CrossRef]
21. Alaoui, O.T.; Nguyen, Q.T.; Mbareck, C.; Rhlalou, T. Elaboration and study of poly (vinylidene fluoride)–anatase TiO_2 composite membranes in photocatalytic degradation of dyes. *Appl. Catal. A Gen.* **2009**, *358*, 13–20. [CrossRef]
22. Rahimpour, A.; Madaeni, S.S.; Taheri, A.H.; Mansourpanah, Y. Coupling TiO_2 nanoparticles with UV irradiation for modification of polyethersulfone ultra filtration membranes. *J. Membr. Sci.* **2008**, *313*, 158–169. [CrossRef]
23. Liu, P.; Liu, H.; Liu, G.; Yao, K.; Lv, W. Preparation of TiO_2 nanotubes coated on polyurethane and study of their photocatalytic activity. *Appl. Surf. Sci.* **2012**, *258*, 9593–9598. [CrossRef]
24. Liu, L.; Chen, F.; Yang, F. Stable photocatalytic activity of immobilized Fe0/TiO_2/ACF on composite membrane in degradation of 2,4-dichlorophenol. *Sep. Purif. Technol.* **2009**, *70*, 173–178. [CrossRef]
25. Rota, F.; Cavassi, M.; Niego, D.; Gorlani, R.; Vianelli, L.; Tatti, L.; Bruzzi, P.; Moroni, A.; Bellobono, I.R.; Bianchi, M.; et al. Mathematical modelling of photomi neralization of phenols in aqueous solution, by photocatalytic membranes immobilizing titanium dioxide. *Chemosphere* **1996**, *33*, 2159–2173. [CrossRef]
26. You, S.-J.; Semblante, G.U.; Lu, S.-C.; Damodar, R.A.; Wei, T.-C. Evaluation of the antifouling and photocatalytic properties of poly(vinylidene fluoride) plasma grafted poly(acrylic acid) membrane with self-assembled TiO_2. *J. Hazard. Mater.* **2012**, *237–238*, 10–19. [CrossRef]
27. Morris, R.E.; Krikanova, E.; Shadman, F. Photocatalytic membrane for removal of organic contaminants during ultra-purification of water. *Clean Technol. Environ. Policy* **2004**, *6*, 96–104. [CrossRef]
28. Wang, K.Y.; Weber, M.; Chung, T.-S. Polybenzimidazoles (PBIs) and state-of-the-art PBI hollow fiber membranes for water, organic solvent and gas separations: A review. *J. Mater. Chem. A* **2022**, *10*, 8687–8718. [CrossRef]
29. Lobato, J.; Cañizares, P.; Rodrigo, M.A.; Úbeda, D.; Javier Pinar, F. A novel titanium PBI-based composite membrane for high temperature PEMFCs. *J. Membr. Sci.* **2011**, *369*, 105–111. [CrossRef]
30. Javier Pinar, F.; Cañizares, P.; Rodrigo, M.A.; Ubeda, D.; Lobato, J. Titanium composite PBI-based membranes for high temperature polymer electrolyte membrane fuel cells. Effect on titanium dioxide amount. *RSC Adv.* **2012**, *2*, 1547–1556. [CrossRef]
31. Díaz-Abad, S.; Rodrigo, M.A.; Sáez, C.; Lobato, J. Enhancement of the Green H_2 Production by Using TiO_2 Composite Polybenzimidazole Membranes. *Nanomaterials* **2022**, *12*, 2920. [CrossRef]
32. Li, Q.; Aili, D.; Hjuler, H.A.; Jensen, J.O. *Editors, High Temperature Polymer Electrolyte Membrane Fuel Cells Approaches, Status, and Perspectives*; Springer International Publishing: Cham, Switzerland, 2016.
33. Murdock, L.A.; Benicewicz, B.C. Preparation of Dense Polybenzimidazole Films without Organic Solvents. *Macromolecules* **2023**, *56*, 2729–2735. [CrossRef]
34. Penchev, H.; Zaharieva, K.; Milenova, K.; Ublekov, F.; Dimova, S.; Budurova, D.; Staneva, M.; Stambolova, I.; Sinigersky, V.; Blaskov, V. Novel meta- and AB-Polybenzimidazole/Zinc oxide polymer hybrid nanomaterials for photocatalytic degradation of organic dyes. *Mater. Lett.* **2018**, *230*, 187–190. [CrossRef]
35. Borisova, D.; Haladjova, E.; Kyulavska, M.; Petrov, P.; Pispas, S.; Stoitsova, S.; Paunova-Krasteva, T. Application of cationic polymer micelles for the dispersal of bacterial biofilms. *Eng. Life Sci.* **2018**, *18*, 943–948. [CrossRef]
36. Paunova-Krasteva, T.; Haladjova, E.; Petrov, P.; Forys, A.; Trzebicka, B.; Topouzova-Hristova, T.; Stoitsova, S.R. Destruction of Pseudomonas aeruginosa pre-formed biofilms by cationic polymer micelles bearing silver nanoparticles. *Biofouling* **2020**, *36*, 679–695. [CrossRef]
37. Paunova-Krasteva, T.; Hemdan, B.A.; Dimitrova, P.D.; Damyanova, T.; El-Feky, A.M.; Elbatanony, M.M.; Stoitsova, S.; Azab El-Liethy, M.; El-Taweel, G.E.; El Nahrawy, A.M. Hybrid Chitosan/CaO-Based Nanocomposites Doped with Plant Extracts from Azadirachta indica and Melia azedarach: Evaluation of Antibacterial and Antibiofilm Activities. *BioNanoSci* **2023**, *13*, 88–102. [CrossRef]
38. Stancheva, R.; Paunova-Krasteva, T.; Topouzova-Hristova, T.; Stoitsova, S.; Petrov, P.; Haladjova, E. Ciprofloxacin-Loaded Mixed Polymeric Micelles as Antibiofilm Agents. *Pharmaceutics* **2023**, *15*, 1147. [CrossRef]
39. Kenawy, E.R.; Worley, S.D.; Broughton, R. The chemistry and applications of antimicrobial polymers: A state-of-the-art review. *Biomacromolecules* **2007**, *8*, 1359–1384. [CrossRef]
40. Chaturvedi, S.; Dave, P.N. Environmental Application of Photocatalysis. *MSF* **2012**, *734*, 273–294. [CrossRef]
41. Priyanka, K.P.; Sukirtha, T.H.; Balakrishna, K.M.; Varghese, T. Microbicidal activity of TiO_2 nanoparticles synthesised by sol-gel method. *IET Nanobiotechnol.* **2016**, *10*, 81–86. [CrossRef]
42. Kőrösi, L.; Pertics, B.; Schneider, G.; Bognár, B.; Kovács, J.; Meynen, V.; Scarpellini, A.; Pasquale, L.; Prato, M. Photocatalytic Inactivation of Plant Pathogenic Bacteria Using TiO_2 Nanoparticles Prepared Hydrothermally. *Nanomaterials* **2020**, *10*, 1730. [CrossRef]

43. Anbumanip, D.; Vizhi Dhandapani, K.; Manoharan, J.; Babujanarthanam, R.; Bashir, A.K.H.; Muthusamy, K.; Alfarhan, A.; Kanimozhi, K. Green synthesis and antimicrobial efficacy of titanium dioxide nanoparticles using Luffa acutangula leaf extract. *J. King Saud Univ. Sci.* **2022**, *34*, 101896. [CrossRef]
44. Serov, D.A.; Gritsaeva, A.V.; Yanbaev, F.M.; Simakin, A.V.; Gudkov, S.V. Review of Antimicrobial Properties of Titanium Dioxide Nanoparticles. *Int. J. Mol. Sci.* **2024**, *25*, 10519. [CrossRef] [PubMed]
45. Sirelkhatim, A.; Mahmud, S.; Seeni, A.; Kaus, N.H.M.; Ann, L.C.; Bakhori, S.K.M.; Hasan, H.; Mohamad, D. Review on Zinc Oxide Nanoparticles: Antibacterial Activity and Toxicity Mechanism. *Nano-Micro Lett.* **2015**, *7*, 219–242. [CrossRef] [PubMed]
46. Kessler, A.; Hedberg, J.; Blomberg, E.; Odnevall, I. Reactive Oxygen Species Formed by Metal and Metal Oxide Nanoparticles in Physiological Media-A Review of Reactions of Importance to Nanotoxicity and Proposal for Categorization. *Nanomaterials* **2022**, *12*, 1922. [CrossRef]
47. Li, Y.; Zhang, W.; Niu, J.; Chen, Y. Mechanism of Photogenerated Reactive Oxygen Species and Correlation with the Antibacterial Properties of Engineered Metal-Oxide Nanoparticles. *ACS Nano* **2012**, *6*, 5164–5173. [CrossRef]
48. Kraus, W.; Nolze, G. *Powder Cell for Windows*; Federal Institute for Materials Research and Testing: Berlin, Germany, 2000.
49. Williams, G.K.; Hall, W.H. X-ray line broadening from filed aluminium and tungsten. *Acta Metall.* **1953**, *1*, 22–31. [CrossRef]
50. Sarker, S.D.; Nahar, L.; Kumarasamy, Y. Microtitre plate-based antibacterial assay incorporating resazurin as an indicator of cell growth, and its application in the in vitro antibacterial screening of phytochemicals. *Methods* **2007**, *42*, 321–324. [CrossRef]
51. Marra, A.; Silvestre, C.; Duraccio, D.; Cimmino, S. Polylactic acid/zinc oxide biocomposite films for food packaging application. *Int. J. Biol. Macromol.* **2016**, *88*, 254–262. [CrossRef]
52. Penchev, H.; Zaharieva, K.; Dimova, S.; Grancharov, G.; Petrov, P.D.; Shipochka, M.; Dimitrov, O.; Lazarkevich, I.; Engibarov, S.; Eneva, R. Hybrid Cellulosic Substrates Impregnated with Meta-PBI-Stabilized Carbon Nanotubes/Plant Extract-Synthesized Zinc Oxide—Antibacterial and Photocatalytic Dye Degradation Study. *Nanomaterials* **2024**, *14*, 1346. [CrossRef]
53. Micic, O.I.; Zhang, Y.; Cromack, K.R.; Trifunac, A.D.; Thurnauer, M.C. Trapped holes on TiO_2 colloids studied by Electron Paramagnetic Resonance. *J. Phys. Chem.* **1993**, *97*, 7277–7283. [CrossRef]
54. Nakaoka, Y.; Nosaka, Y. ESR investigation into the effects of heat treatment and crystal structure on radicals produced over irradiated TiO_2 powder. *J. Photochem. Photobiol. A Chem.* **1997**, *110*, 299–305. [CrossRef]
55. Kumar, C.P.; Gopal, N.O.; Wang, T.C.; Wong, M.-S.; Ke, S.C. EPR investigation of TiO_2 nanoparticles with temperature-dependent properties. *J. Phys. Chem. B* **2006**, *110*, 5223–5229. [CrossRef] [PubMed]
56. Liu, D.; Chen, D.; Li, N.; Xu, Q.; Li, H.; He, J.; Lu, J. Surface engineering of g-C_3N_4 by stacked Bi-OBr sheets rich in oxygen vacancies for boosting photoctalytic performance. *Angew. Chem. Int. Ed. Engl.* **2020**, *59*, 4519–4524. [CrossRef] [PubMed]
57. Asensio, J.A.; Gomez-Romero, P. Recent developments on proton conducting poly(2,5- ben-zimidazole) ABPBI membranes for high temperature polymer electrolyte membrane fuel cells. *Fuel Cell.* **2005**, *5*, 336–343. [CrossRef]
58. Arlt, T.; Lüke, W.; Kardjilov, N.; Banhart, J.; Lehnert, W. Monitoring the hydrogen distribution in poly(2,5- benzimidazole) based membranes in operating high-temperature polymer electrolyte fuel cells by using H-D contrast neutron imaging. *J. Power Sources* **2015**, *299*, 125–129. [CrossRef]
59. Vogel, H.; Marvel, C.S. Polybenzimidazoles, new thermally stable polymers. *J. Polym. Sci.* **1961**, *50*, 511–539. [CrossRef]
60. Perry, K.A.; Eisman, G.A.; Benicewicz, B.C. Electrochemical hydrogen pumping using a high-temperature polybenzimidazole (PBI) membrane. *J. Power Sources* **2008**, *177*, 478–484. [CrossRef]
61. Xiao, L.; Zhang, H.; Scanlon, E.; Ramanathan, L.S.; Choe, E.-W.; Rogers, D.; Apple, T.; Benicewicz, B.C. High-Temperature Polybenzimidazole Fuel Cell Membranes via a Sol-Gel Process. *Chem. Mater.* **2005**, *17*, 5328–5333. [CrossRef]
62. Zhou, D.; Ji, Z.; Jiang, X.; Dunphy, D.R.; Brinker, J.; Kel-ler, A.A. Influence of material properties on TiO_2 nanoparticle agglomeration. *PLoS ONE* **2013**, *8*, e81239. [CrossRef]
63. Lu, Y.; Zhou, S.; Wu, L. De-Agglomeration and Dispersion Behaviour of TiO_2 Nanoparticles in Organic Media Using 3-Methacryloxypropyltrimethoxysilane as a Surface Modifier. *J. Dispers. Sci. Technol.* **2012**, *33*, 497–505. [CrossRef]
64. Lohokare, H.R.; Chaudhari, H.D.; Kharul, U.K. Solvent and pH-stable poly(2,5-benzimidazole) (ABPBI) based UF membranes: Preparation and characterizations. *J. Membr. Sci.* **2018**, *563*, 743–751. [CrossRef]
65. Brunel, R.; Marestin, C.; Martin, V.; Mercier, R. Water-Borne Polyimides via Microwave-Assisted Polymerization. *High Perform. Polym.* **2010**, *22*, 82–94. [CrossRef]
66. Yang, J.; He, R.; Che, Q.; Gao, X.; Shi, L. A Copolymer of Poly[2,20-(m-Phenylene)-5,50- Bibenzimidaz-ole] and Poly(2,5-Benzimidazole) for High-Temperature Proton-Conducting Membranes. *Polym. Int.* **2010**, *59*, 1695–1700. [CrossRef]
67. Olvera-Mancilla, J.; Palacios-Alquisira, J.; Escobar-Barrios, V.A.; Alexandrova, L. Some aspects of polybenzimidazoles' synthesis in Eaton reagent under different temperatures and microwave irradiation. *J. Macromol. Sci. Part A Pure Appl. Chem.* **2019**, *56*, 609–617. [CrossRef]
68. Chaudhari, H.D.; Illathvalappil, R.; Kurungot, S.; Kharul, U.K. Preparation and investigations of ABPBI membrane for HT-PEMFC by immersion precipitation method. *J. Membr. Sci.* **2018**, *564*, 211–217. [CrossRef]
69. Bhatti, M.A.; Tahira, A.; Chandio, A.d.; Almani, K.F.; Bhatti, A.L.; Waryani, B.; Nafady, A.; Ibupoto, Z.H. Enzymes and phytochemicals from neem extract robustly tuned the photocatalytic activity of ZnO for the degradation of malachite green (MG) in aqueous media. *Res. Chem. Intermed.* **2021**, *47*, 1581–1599. [CrossRef]

70. Song, C.; Jiao, Y.; Tian, Z.; Qin, Q.; Qin, S.; Zhang, J.; Li, J.; Cui, Z. Fabrication of hollow-fiber nanofiltration membrane with negative-positive dual-charged separation layer to remove low concentration $CuSO_4$. *Sep. Purif. Technol.* **2022**, *296*, 121352. [CrossRef]
71. Coppola, R.E.; Lozano, H.E.; Contin, M.; Canneva, A.; Mo-linari, F.N.; Abuinaan, G.C.; D'Accorso, N.B. Polybenzimidazole membrane for efficient copper removal from aqueous solutions. *Polym. Int.* **2022**, *71*, 1143–1151. [CrossRef]
72. Andreeva, R.; Stoyanova, E.; Tsanev, A.; Stoychev, D. Influence of the Pre-Treatment and Post-Treatment Operations on the Surface Chemistry and Corrosion Behavior of Cerium-Based Conversion Coatings on Aluminum. *Curr. Adv. Chem. Bio-Chem.* **2021**, *7*, 1–28. [CrossRef]
73. Bianchi, C.L.; Cappelletti, G.; Ardizzone, S.; Gialanella, S.; Naldoni, A.; Oliva, C.; Pirola, C. N-doped TiO_2 from $TiCl_3$ for photodegradation of air pollutants. *Catal. Today* **2009**, *144*, 31–36. [CrossRef]
74. Wang, Y.; Feng, C.; Zhang, M.; Yang, J.; Zhang, Z. Enhanced visible light photocatalytic activity of N-doped TiO_2 in relation to single-electron-trapped oxygen vacancy and doped-nitrogen. *Appl. Catal. B Environ.* **2010**, *100*, 84–90. [CrossRef]
75. Giannakas, A.E.; Seristatidou, E.; Deligiannakis, Y.; Konstantinou, I. Photocatalytic activity of N-doped and N-F co-doped TiO_2 and reduction of chromium (VI) in aqueous solution: An EPR study. *Appl. Catal. B Environ.* **2013**, *132–133*, 460–468. [CrossRef]
76. Khade, G.V.; Suwarnkar, M.B.; Gavade, N.L.; Garadkar, K.M. Green synthesis of TiO_2 and its photocatalytic activity. *J. Mater. Sci. Mater. Electron.* **2015**, *26*, 3309–3315. [CrossRef]
77. Senthilkumar, S.; Ashok, M.; Kashinath, L.; Sanjeeviraja, C.; Rajendran, A. Phytosynthesis and Characterization of TiO_2 Nanoparticles using Diospyros ebenum Leaf Extract and their Antibacterial and Photocatalytic Degradation of Crystal Violet. *Smart Sci.* **2017**, *6*, 1–9. [CrossRef]
78. Zeng, L.; Zhao, T.; An, L.; Zhao, G.; Yan, X. Physicochemical properties of alkaline doped polybenzimidazole membranes for anion exchange membrane fuel cells. *J. Membr. Sci.* **2015**, *493*, 340–348. [CrossRef]
79. Kumbharkar, S.C.; Islam, M.N.; Potrekar, R.A.; Kharul, U.K. Variation in acid moiety of polybenzimidazoles: Investigation of physico-chemical properties towards their applicability as proton exchange and gas separation membrane materials. *Polymer* **2009**, *50*, 1403–1413. [CrossRef]
80. Kumbharkar, S.C.; Kharul, U.K. New N-substituted ABPBI: Synthesis and evaluation of gas permeation properties. *J. Membr. Sci.* **2010**, *360*, 418–425. [CrossRef]
81. Tian, Z.; Wang, S.; Wu, Y.; Yan, F.; Qin, S.; Yang, J.; Li, J.; Cui, Z. Fabrication of polymer@TiO_2 NPs hybrid membrane based on covalent bonding and coordination and its mechanism of enhancing photocatalytic performance. *J. Alloys Compd.* **2022**, *910*, 164887. [CrossRef]
82. Lou, L.; Kendall, R.J.; Ramkumar, S. Comparison of hydrophilic PVA/TiO_2 and hydrophobic PVDF/TiO_2 microfiber webs on the dye pollutant photo-catalyzation. *J. Environ. Chem. Eng.* **2020**, *8*, 103914. [CrossRef]
83. Jumat, N.A.; Wai, P.S.; Ching, J.J.; Basirun, W.J. Synthesis of Polyaniline-TiO_2 nanocomposites and their Application in Photocatalytic degradation. *Polym. Polym. Compos.* **2017**, *25*, 507–513. [CrossRef]
84. Sangareswari, M.; Sundaram, M.M. Development of efficiency improved polymer-modified TiO_2 for the photocatalytic degradation of an organic dye from wastewater environment. *Appl. Water Sci.* **2017**, *7*, 1781–1790. [CrossRef]
85. Shah, L.A.; Malik, T.; Siddiq, M.; Haleem, A.; Sayed, M.; Naeem, A. TiO_2 nanotubes doped poly(vinylidene fluoride) polymer membranes (PVDF/TNT) for efficient photocatalytic degradation of brilliant green dye. *J. Environ. Chem. Eng.* **2019**, *7*, 103291. [CrossRef]
86. Song, L.; Qiu, R.; Mo, Y.; Zhang, D.; Wei, H.; Xiong, Y. Photodegradation of phenol in a polymer-modified TiO_2 semiconductor particulate system under the irradiation of visible light. *Catal. Commun.* **2007**, *8*, 429–433. [CrossRef]
87. Xiong, L.; Ouyang, M.; Yan, L.; Li, J.; Qiu, M.; Yu, Y. Visible-light energy storage by Ti^{3+} in TiO_2/Cu_2O bilayer film. *Chem. Lett.* **2009**, *38*, 1154–1155. [CrossRef]
88. Xing, M.; Zhang, J.; Chen, F.; Tian, B. An economic method to prepare vacuum activated photocatalysts with high photo-activities and photosensitivities. *Chem. Commun.* **2011**, *47*, 4947–4949. [CrossRef]
89. Chakansin, C.; Yostaworakul, J.; Warin, C.; Kulthong, K.; Boonrungsiman, S. Resazurin rapid screening for antibacterial activities of organic and inorganic nanoparticles: Potential, limitations and precautions. *Anal. Biochem.* **2022**, *637*, 114449. [CrossRef]
90. Akhtar, S.; Ali, I.; Tauseef, S. Synthesis, characterization and antibacterial activity of titanium dioxide (TiO_2) nanoparticles. *FUUAST J. Biol.* **2016**, *6*, 141–147.
91. Anandgaonker, P.; Kulkarni, G.; Gaikwad, S.; Rajbhoj, A. Synthesis of TiO_2 nanoparticles by electrochemical method and their antibacterial application. *Arab. J. Chem.* **2019**, *12*, 1815–1822. [CrossRef]
92. Rathi, V.; Rejo Jeice, A. Green fabrication of titanium dioxide nanoparticles and their applications in photocatalytic dye degradation and microbial activities. *Chem. Phys. Impact* **2023**, *6*, 100197. [CrossRef]
93. Arora, B.; Murar, M.; Dhumale, V. Antimicrobial potential of TiO_2 nanoparticles against MDR Pseudomonas aeruginosa. *J. Exp. Nanosci.* **2014**, *10*, 819–827. [CrossRef]
94. Kassalia, M.-E.; Chorianopoulos, N.; Nychas, G.-J.; Pavlatou, E.A. Investigation of the Photoinduced Antimicrobial Properties of N-Doped TiO_2 Nanoparticles under Visible-Light Irradiation on Salmonella Typhimurium Biofilm. *Appl. Sci.* **2023**, *13*, 4498. [CrossRef]

95. Damyanova, T.; Dimitrova, P.; Borisova, D.; Topouzova-Hristova, T.; Haladjova, E.; Paunova-Krasteva, T. An overview of biofilm-associated infections and the role of phytochemicals and nanomaterials in their control and prevention. *Pharmaceutics* **2024**, *16*, 162. [CrossRef] [PubMed]
96. Saito, T.; Iwase, T.; Horie, J.; Morioka, T. Mode of photocatalytic bactericidal action of powdered semiconductor TiO_2 on mutans streptococci. *J. Photochem. Photobiol. B* **1992**, *14*, 369–379. [CrossRef] [PubMed]
97. Zhang, L.; Wu, L.; Si, Y.; Shu, K. Size-Dependent Cytotoxicity of Silver Nanoparticles to Azotobacter Vinelandii: Growth Inhibition, Cell Injury, Oxidative Stress and Internalization. *PLoS ONE* **2018**, *13*, e0209020. [CrossRef] [PubMed]

Disclaimer/Publisher's Note: The statements, opinions and data contained in all publications are solely those of the individual author(s) and contributor(s) and not of MDPI and/or the editor(s). MDPI and/or the editor(s) disclaim responsibility for any injury to people or property resulting from any ideas, methods, instructions or products referred to in the content.